N O T I C E

THIS DOCUMENT HAS BEEN REPRODUCED FROM
MICROFICHE. ALTHOUGH IT IS RECOGNIZED THAT
CERTAIN PORTIONS ARE ILLEGIBLE, IT IS BEING RELEASED
IN THE INTEREST OF MAKING AVAILABLE AS MUCH
INFORMATION AS POSSIBLE

NASA

DESIGN, FABRICATION AND TESTING OF AN OPTICAL TEMPERATURE SENSOR

by W.W. Morey, W.H. Glenn,
R.O. Decker and W.C. McClurg

UNITED TECHNOLOGIES RESEARCH CENTER

prepared for

NATIONAL AERONAUTICS AND SPACE ADMINISTRATION

NASA Lewis Research Center

NASA

DESIGN, FABRICATION AND TESTING OF AN OPTICAL TEMPERATURE SENSOR

by W.W. Morey, W.H. Glenn,
R.O. Decker and W.C. McClurg

UNITED TECHNOLOGIES RESEARCH CENTER

prepared for

NATIONAL AERONAUTICS AND SPACE ADMINISTRATION

1. Report No.	2. Government Accession No.	3. Recipient's Catalog No.
NASA CR-165125		
4. Title and Subtitle		5. Report Date
Design, Fabrication and Testing of an Optical Temperature Sensor		July 1980
		6. Performing Organization Code
7. Author(s)		8. Performing Organization Report No.
W. W. Morey, W. H. Glenn, R. O. Decker, W. C. McClurg		R80-924625-11
		10. Work Unit No.
9. Performing Organization Name and Address		
United Technologies Research Center		
400 Main Street		11. Contract or Grant No.
East Hartford, CT 06108		NAS3-21841
		13. Type of Report and Period Covered
12. Sponsoring Agency Name and Address		Contractor report
National Aeronautics and Space Administration		
Lewis Research Center		14. Sponsoring Agency Code
21000 Brookpark Raod, Cleveland, OH 44135		

15. Supplementary Notes

16. Abstract

The objective of the program reported here was to design, fabricate, and test a laboratory breadboard optical temperature sensor based on the temperature dependent absorptive characteristics of a rare earth (europium) doped optical fiber. This concept arose as a result of a study carried out under a previous NASA program, Contract NAS3-21004. The report discusses the principles of operation, materials characterization, fiber and optical component design, design and fabrication of an electro-optic interface unit, signal processing, and initial test results. The initial tests indicated that, after a brief warmup period, the output of the sensor was stable to approximately $1°C$ at room temperature or approximately ± 0.3 percent of point ($°K$). This exceeds the goal of 1 percent of point. Recommendations are presented for further performance improvement.

17. Key Words (Suggested by Author(s))		18. Distribution Statement	
Optical Temperature Sensor			
19. Security Classif. (of this report)	20. Security Classif. (of this page)	21. No. of Pages	22. Price*
Unclassified	Unclassified	50	

NASA-C-168 (Rev. 6-71)

Analysis and Preliminary Design of Optical Sensors for Propulsion Control

TABLE OF CONTENTS

SUMMARY

The objective of the program reported here was to design, fabricate, and test a laboratory breadboard optical temperature sensor based on the temperature dependent absorptive characteristics of a rare earth (europrium) doped optical fiber. This concept arose as a result of a study carried out under a previous NASA program, Contract NAS3-21004. The report discusses the principles of operation, materials characterization, fiber and optical component design, design and fabrication of an electro-optic interface unit, signal processing, and initial test results. The initial tests indicated that, after a brief warmup period, the output of the sensor was stable to approximately 1°C at room temperature or approximately $\pm$ 0.3 percent of point (°K). This exceeds the goal of 1 percent of point. Recommendations are presented for further performance improvement.

1. INTRODUCTION

The objective of the program reported here was to conduct further analysis and preliminary design of an optical temperature sensor based on the temperature dependent absorption characteristics of a rare earth doped optical fiber. This approach arose as a result of a concept screening study that was carried out under a previous NASA program. Of the several approaches that emerged from the study, the rare earth probe was selected as the most promising for further development.

The reasoning that led to the idea of the rare earth probe can be summarized as follows:

(a) Rare earth ions have numerous absorption lines in the visible and near IR portion of the spectrum. The transmission of a sample can be monitored at selected wavelength with commercially available LED's or laser diodes.

(b) Some of the absorption lines correspond to optical transitions that originate in the ground electronic state of the ion while others are transitions that originate in low lying excited levels. The strength of an absorption is proportional to the population of ions in the state from which the absorbing transition originates. The population distribution is a unique function of temperature. In general, transitions originating in the ground state should show a decrease in strength with increasing temperature due to depletion of the ground state population. Transitions originating in higher states should show an increase in strength with temperature due to the increase of the population. Either type of absorption may be used to monitor the temperature, or they may be used in combination for increased sensitivity.

(c) Rare earth ions may readily be incorporated into a glass or crystalline host material and the resulting material can be made with very good optical quality. (Doping of glass and crystals with neodymium has been extensively developed for the production of laser rods. The chemistry of all the rare earth elements is similar to that of neodymium.) Rare earth doped glass may readily be drawn into optical fibers by standard techniques. A rare earth sensor can be made with an active sensing element consisting of either a rare earth doped bulk sample or a rare earth doped fiber.

These considerations form the basis of the rare earth temperature probe. In implementing the concept, some additional considerations are:

(a) The measured transmission should be independent of the intensity of the light source used to make the measurement. This requires either that the source intensity be maintained constant, or that both input and output intensity be measured and ratioed to remove the dependence on source intensity.

(b) It is desirable that the final measured output that is used to determine the temperature be independent of incidental losses such as would be caused by changing cables or connectors leading from the sensor head to the electronic interface unit. One approach to achieving this independence is through the use of a reference beam at a different wavelength from the sensing beam. The wavelength of the reference beam may be chosen to lie in a region where the rare earth has no absorption. The transmission of the reference beam then monitors the transmission of the fiber heads, connectors, etc., and can be used to normalize this factor out of the transmission of the sensing beam. It is not necessary that the reference beam be at a wavelength where the rare earth is not absorbing. It need only be at a wavelength where the absorption has a different temperature dependence. In this case there are really two sensing beams; one could monitor an absorption that increases with temperature and the other an absorption that decreases with temperature. The ratio of the two transmission is independent of the incidental losses provided that they are wavelength independent.

(c) If the signal and reference beams are detected by a single detector, drifts in detector sensitivity are also ratioed out. This could be a problem if separate detectors were used. Use of a single detector requires either time or frequency multiplexing of the two beams.

(d) The ultimate accuracy of the temperature measurements depends on the rate of change of the measured transmission ratio with temperature (i.e., sensitivity) and the accuracy with which a given transmission ratio can be measured (i.e., signal-to-noise ratio). The latter depends on the amount of light available at the detector. This in turn depends on the source intensity and the absorption of the sensor head and leads. It may be shown that for a given source intensity there is an optimum absorption length, so that the signal-to-noise ultimately depends on the source intensity. In selecting the wavelength for the sensing beam (or beams) one must choose a wavelength at which the absorption changes rapidly with the temperature and for which sufficiently intense sources are available.

These are the general considerations for the design of the temperature probe. The following sections will discuss choice of materials, fiber fabrication, design and fabrication of the electro-optic interface, optical component fabrication, and signal processing. The present state of development will be reviewed and recommendations made for further development.

2. CHOICE OF MATERIALS FOR THE SENSOR

2.1 General Considerations

In the previous section, reasons were given for the choice of rare earth elements for the temperature probe. Figure 2-1 shows the energy levels for the trivalent rare earths in a crystalline host, $LaCl_3$. The funtion of the energy levels of the rare earths are not strongly dependent on the host so that one would expect a qualitatively similar picture for a glass host. The energy levels in this figure are plotted versus wavenumber (cm^{-1}). At a temperature, T, one would expect significant population of levels up to a few times kT above the ground state. We may express kT in terms of wavenumber by the relation:

$$kT = h\nu = \frac{hc}{\lambda}$$

$$\frac{1}{\lambda} = \frac{kT}{hc}$$

$$= 0.692 \ T \quad T \ in \ ^\circ K$$

$$= 0.385 \ T \quad T \ in \ ^\circ R$$

Thus, for a temperature of $2500^\circ R = 1388^\circ K$, $1/\lambda = 962 \ cm^{-1}$. For measurement of temperature below this value, then it would be desirable to have a rare earth ion with energy levels below or not far above $962 \ cm^{-1}$. Inspection of this level diagram will show that europioum (Eu) and samarium (Sm) are the most promising candidates with cerium (Ce), prascodymium (Pr), neodymium (Nd), promethium (Pm) and terbium (Tb) as other potential candidates, particularly at high temperatures. (Promethium, however, is radioactive and extremely rare; terbium is also extremely rare so that these two elements should be excluded.) Europium is particularly attractive due to its very low lying levels and the fact that there are several useful levels.

Some preliminary data were taken on the temperature dependent absorption of both europium- and samarium-doped glasses. The europium data appeared more promising as there were well defined absorption peaks that varied with temperature. The absorption spectrum of the samarium was more complicated and did not vary with temperature in as well defined a way. (Considerable broadening of levels and washing out of the structure was observed.) For this reason, europium was chosen as the prime candidates and more detailed consideration was confined to this ion. Figure 2-2 shows the lowest energy levels of europium in more detail. From this we can see that there should be two major sets of absorption peaks, one set arising from transitions originating in one of the low lying states and terminating in the $^5D_0$ state and the other originating in the lower states and terminating in the $^5D_1$ state.

From this energy level structure we may calculate the expected distribution of population in the lower states as a function of temperature. At this point it will be valuable to review the significance of the spectroscopic notation. The letter

FIG. 2.1

ENERGY LEVEL DIAGRAMS FOR TRIVALENT RARE EARTHS IN LaCl₃

4

FIG. 2.2

THE ENERGY LEVEL DIAGRAM FOR Eu^{3+} IN GLASS. THE SPLITTING ASSOCIATED WITH
THE J MULTIPLICITY (M = 2J + 1) IS SHOWN.

78-07-138-2

5
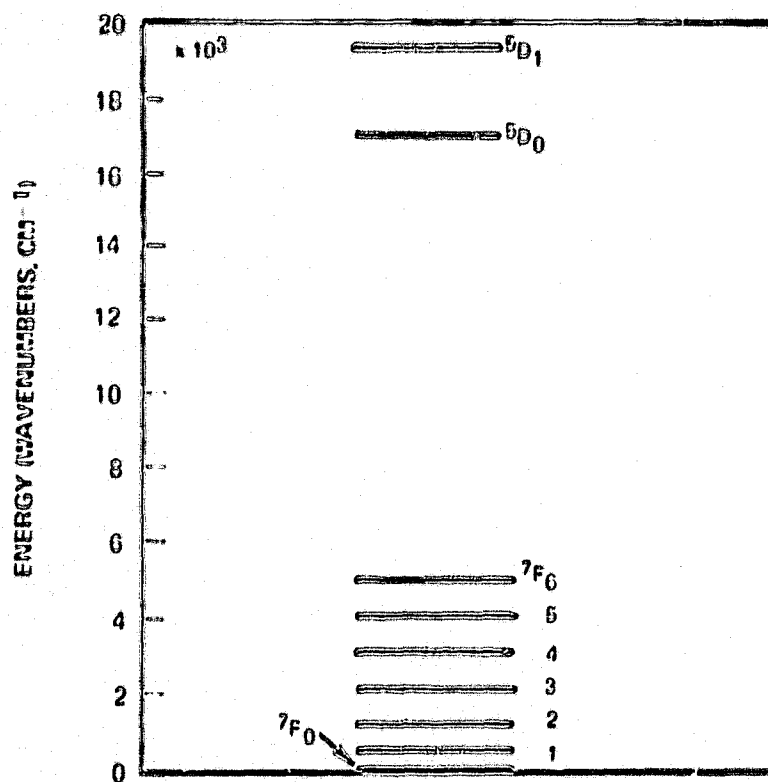
designation refers to the total orbital angular momentum, $\bar{L}$, of the electrons
(S = 0, P = 1, D = 2, F = 3, G = 4, H = 5, I = 6, etc.). Thus the F states have
an orbital angular momentum of 3. The superscript refers to the total spin angular
momentum. If the total spin angular momentum is s, then the superscript is 2s+1.
Thus, for a ^{7}F configuration the total spin is also 3 (7 = 2 x 3 + 1). The spin
and the orbital angular momentum couple together to give the total angular momentum
J. The subscript gives the value of J. A spin of 3 and an orbital angular momentum
of 3 can couple together to give a total angular momentum of J = 0, 1, 2, 3, 4, 5,
or 6. This is the origin of the seven lowest energy levels of the europium ion.
These states are not actually single states but are degenerate because of the
various possible spatial orientation of the total angular momentum J. For a given
value of J, there are 2J+1 possible orientations. Thus, the F_0 state is a singlet,
the F_1 is threefold degenerate, the F_2 is fivefold degenerate, etc. This J
degeneracy is a result of the crystal symmetry. In other hosts, it may be split
by the local field seen by the ion.

We may now calculate the expected distribution of population in the ^{7}F states
as a function of temperature, assuming thermodynamic equilibrium. These states are
the only ones that will have any significant thermal population, and the rest of
the states may be ignored. The population n_J of the Jth state (i.e., the ^{7}F state
with subscript J) is given by

$$n_J = n_0 \; \frac{(2J+1)e^{\frac{-\Delta E_J}{kT}}}{\sum\limits_{J=0}^{6} (2J+1)e^{\frac{-\Delta E_J}{kT}}} \qquad (2\text{-}1)$$

The (2J+1) factor arises from the multiplicity of the levels that was discussed
above. The quantity n_0 is the total number density (cm^{-3}) of ions in the glass.
The population values may be calculated numerically, and the result is shown in
Fig. 2-3. In this calculation the energy level spacings were taken as 421, 987,
2000, 3000 and 4000 cm^{-1}. Including the ^{7}F$_6$ state at x 5000 cm^{-1} was found to have
negligible effect.

This figure shows several interesting features. The population of the ground
state decreases monotonically with temperature. Absorption lines originating in
this state should thus become weaker with increasing temperature. Over most of the
temperature range of interest, the population of the first state is not a strong
function of temperature; absorption lines originating in this state should be only
weakly temperature dependent. The next (^{7}F$_2$) state shows a population that increases
monotonically over the temperature range of interest. Absorption lines originating
in this state should increase in strength as the temperature increases.

The model for the population distribution may be used to determine the optimum
path length and transition for use in a temperature sensor. We consider the optical

FIG. 2.3

POPULATION OF GROUND STATE MANIFOLD OF Eu^{3+}
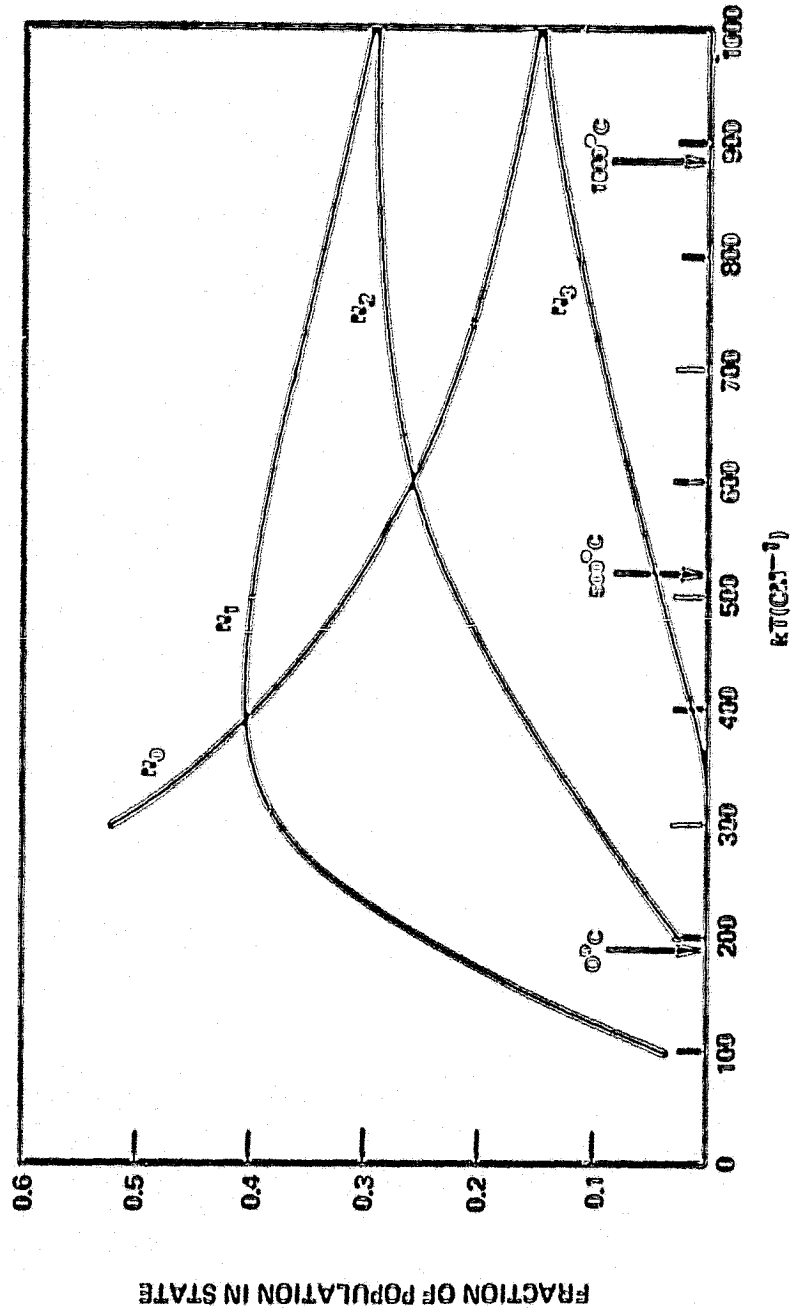
the optical transmission of a glass sample at a wavelength corresponding to one of the absorption peaks. The optical power P that will be transmitted is related to the incident power P_0 by

$$P = P_0 e^{-n_J \sigma_J \ell}$$

Here n_J is the population density of the initial state of the transition, σ_J is the absorption cross section and ℓ is the path length. The temperature sensitivity of the optical transmission may be calculated as

$$\frac{d}{dT} \frac{P}{P_0} = - \sigma_J \ell \frac{dn_J}{dT} e^{-n_J \sigma_J \ell}$$

and from the previously given expression for n_J, we may calculate

$$\frac{dn_J}{dT} = \frac{n_0(2J+1) \frac{\Delta E_J}{kT^2}}{Z} - \frac{n_0(2J+1) \sum (2J+1) \frac{\Delta E_J}{kT^2} e^{-\frac{\Delta E_J}{kT}}}{Z^2} \tag{2-2}$$

here Z is the partition function (the denominator of Eq. (2-1)). This may be simplified to

$$\frac{dn_J}{dT} = n_J \frac{\Delta E_J - <\Delta E>}{kT^2} \tag{2-3}$$

where

$$<\Delta E> = \frac{\sum_J (2J+1) \Delta E_J \; e^{-\frac{\Delta E_J}{kT}}}{Z} \tag{2-4}$$

is just the average energy at a temperature T (which will be comparable to kT). The temperature sensitivity is then

$$\frac{d}{dT} \frac{P}{P_0} = - n_J \sigma \ell \; e^{-n_J \sigma_J \ell} \frac{\Delta E_J - <\Delta E>}{kT^2} \tag{2-5}$$

Regarded as a function of $n_J \sigma_J \ell$, this sensitivity is maximized when $n_J \sigma_J \ell = 1$ or when the transmission P/P_0 is just e^{-1}. The path length in the sensor element should therefore be chosen so that the transmission (say at the center of the range) is e^{-1}. The transmission can also be varied by changing the doping density n_0. It is also desirable to make the magnitude of $\Delta E_J - <\Delta E>$ as large as possible. This indicates

that we should choose a transition originating either in the ground state, for which $\Delta E_J \simeq 0$, or in a highly excited state with a large ΔE_J. A particularly poor choice is a transition originating in a state for which $\Delta E_J \approx \langle \Delta E \rangle$. This is the case for transition originating in the $^7F_1$ state. The above expression predicts a weak temperature dependence which is just a reflection of the weak dependence of the population shown in Fig. 2-3.

## 2.2 Preliminary Measurements of the Temperature Dependent Absorption in Europium

The general considerations discussed above led to the choice of europium for the temperature sensor. A sample ($\sim$ 10 lbs) of europium-doped glass was prepared by Emdex, West Haven, CT. This glass was a high expansion borosilicate glass similar to EN1 and contained 15 percent Eu_2O_3. This glass was prepared under oxidizing conditions to ensure that all the europium was in the Eu^{3+} state. If this is not done, some of the europium will be in the Eu^{2+} state. This leads to an undesirable background absorption that does not vary strongly with temperature. Glass containing only Eu^{3+} ions is a pale pink color; the presence of Eu^{2+} leads to a straw color. The sample of glass obtained from Emdex appeared to be free of any significant amount of Eu^{2+}. Approximately 300 meters of optical fiber with a europium-doped core and an EN1 glass cladding were also obtained from Emdex. This fiber was used for some initial measurements, but most work was done with fibers that were fabricated at UTRC from the bulk sample.

Figure 2-4 shows the typical temperature dependent absorption of a europium-doped fiber. These data were taken with a scanning monochrometer and a photomultiplier. Three prominent absorptions occur at wavelengths of approximately 570 nm, 580 nm, and 605 nm. These correspond to the $7F_0-^5D_0$, $7F_1-^5D_0$ and $7F_2-^5D_0$ transition, respectively. These are also three peaks at shorter wavelength (only two are shown in the figure). Then correspond to transitions from the same initial states to the ^5D state.

The behavior of the absorption with increasing temperature is qualitatively as expected from the calculation of Fig. 2-3. The $7F_0-^5D_0$ transition decreases in strength due to depletion of the $^7D_0$ ground state population. The $7F_2-^5D_0$ transition increases in strength due to the increase in population of the $^7F_2$ state. The $^7F_1-^5D_0$ transition does not vary much as would be expected from Fig. 2-3. The fallout in the signal at long wavelengths is due to the response of the photomultiplier that was used. The fiber is actually clear in this region.

In order to simulate the results that would be obtained from an actual sensor, the transmission was maintained as a function of temperature at two specific wavelengths. The results are shown in Fig. 2-5. The MV5052 LED had a peak emission centered at about 670 nm, in a clear region of the fiber. The transmission at this
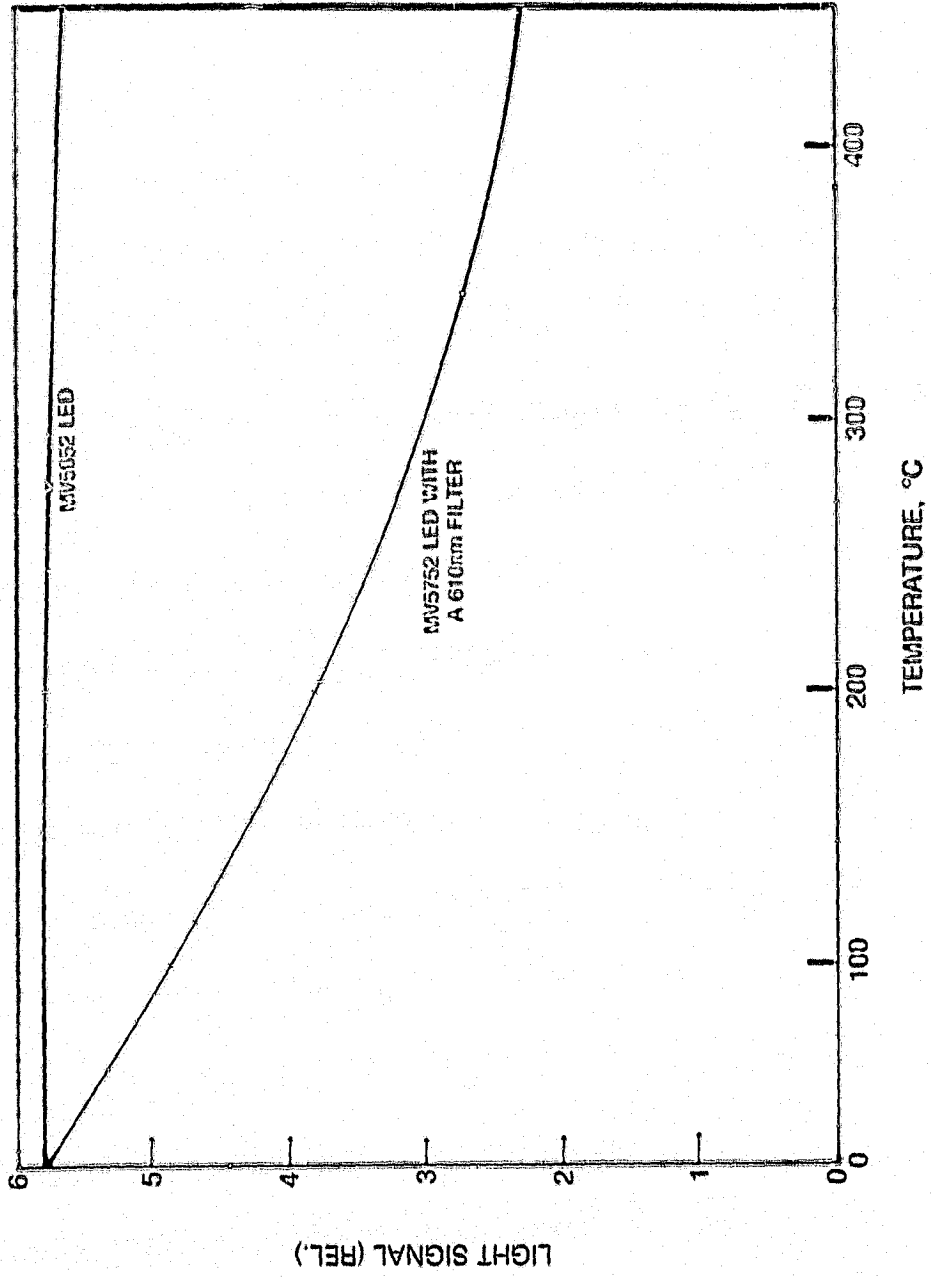
TRANSMISSION OF EUROPIUM DOPED FIBER AT DIFFERENT TEMPERATURES VS WAVELENGTH

70-07-3-1

FIG. 2.5
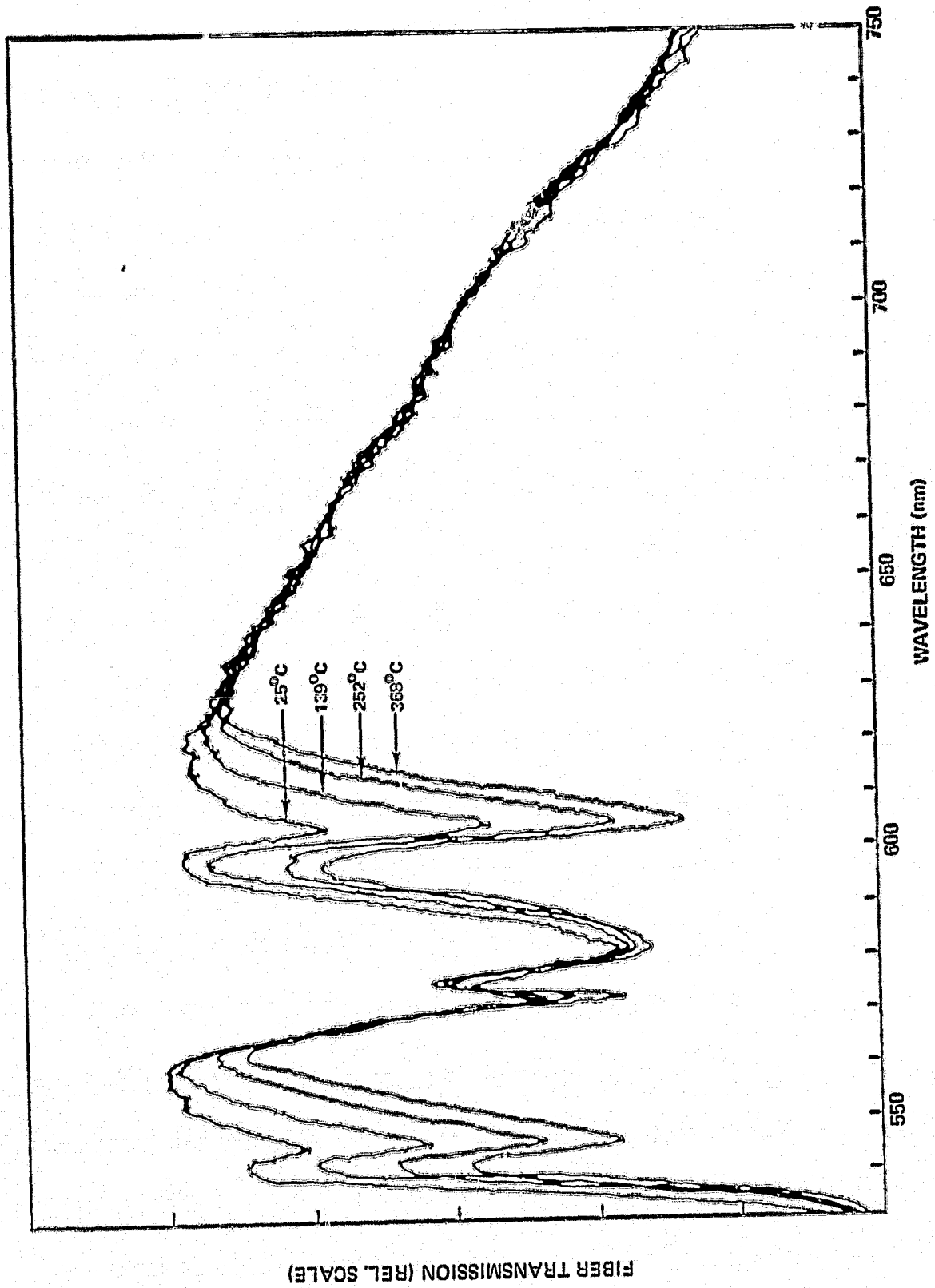
LIGHT INTENSITY TRANSMITTED BY TEMPERATURE SENSING FIBER

MV5052 LED

MV5752 LED WITH
A 610nm FILTER

TEMPERATURE, °C

LIGHT SIGNAL (REL.)

wavelength is virtually independent of temperature. An MV5752 LED with a 610 nm interference filter was used to monitor the $^7F_1$-$^5D_0$ transmission. The transmitted signal fell off approximately exponentially with temperature.

The preliminary data appeared very promising and work was begun to design and fabricate the prototype sensor discussed in the following sections.

3. DESIGN OF OPTICS MODULE AND SENSOR HEAD

3.1 Introduction

As discussed above, the fiber-optic temperature sensor works on the principle of temperature dependent absorption in a rare earth-doped glass. The measurable parameter is a change in power of an optical signal passing through the europium-doped fiber. If there are other effects besides temperature that change the optical power, then an absolute temperature cannot be determined. For instance, a fiber connector that is unmated and remated may cause a small but significant change in optical power transmitted through the fiber, which could be interpreted as a change in temperature. We can eliminate this kind of an error by sending a second optical signal through the same fiber. The wavelength of the second signal is chosen to lie in a portion of the spectrum where there is no temperature dependent absorption. By taking the ratio of the two signals, we measure the transmission of the fiber which varies with temperature and is independent of the optical power in the fiber.

Light emitting diodes (LED's) were chosen as the light source for the temperature sensor. LED's have advantages over an incandescent light including small size, high brightness, high efficiency, and they have the ability of being modulated at reasonably high rates. Laser diodes can couple more than ten times the amount of optical power into fibers than LED's, but there are no laser diodes on the market that emit at the required wavelengths for the europium fiber sensor; and, in general, laser diodes are considerably more expensive than LED's. In order to obtain sufficient wavelength separation, two separate LED's were used. We are then required to couple both otpical sources into a single fiber. This was accomplished using a four-port fiber coupler.

To avoid errors caused by changes in the intensities of the two diodes, an additional reference signal is extracted with the four port coupler and the sensor signal levels are normalized to the reference levels. Normally, four photo-detectors would be required: two detectors for each wavelength for the reference signals, and two detectors for each wavelength for the signals that pass through the sensing fiber. A dispersive element or bandpass filter at each detector would be required. By modulating the two LED's on and off alternately, we can sample both wavelengths at different times. This method of time domain multiplexing reduces the number of detectors to two and was chosen as the detection scheme for the temperature sensor.

We considered several different sensor head designs. The required length of europium fiber is about 15 cm to obtain a 1/e absorption at an intermediate temperature. We will show later that this absorption length is optimum for the best sensitivity. We chose to use a continuous loop of feber for the sensor with a 5 cm radius. A single fiber with an end reflector could also be used, but this sensor gesign gives

a background of reflected light from the various fiber junctions, connections, and splices. In addition, a separation of the incident and return optical signals is required at the input end of the fiber, and this would give an additional 3 dB loss. A single ended temperature probe configuration could also be made by making a very small radius, 180° (i.e., folded back) bend in the fiber. We have constructed 180° fiber bends as small as 0.56 mm radius and have measured transmission losses through these bends of less than 2dB (Ref. 1).
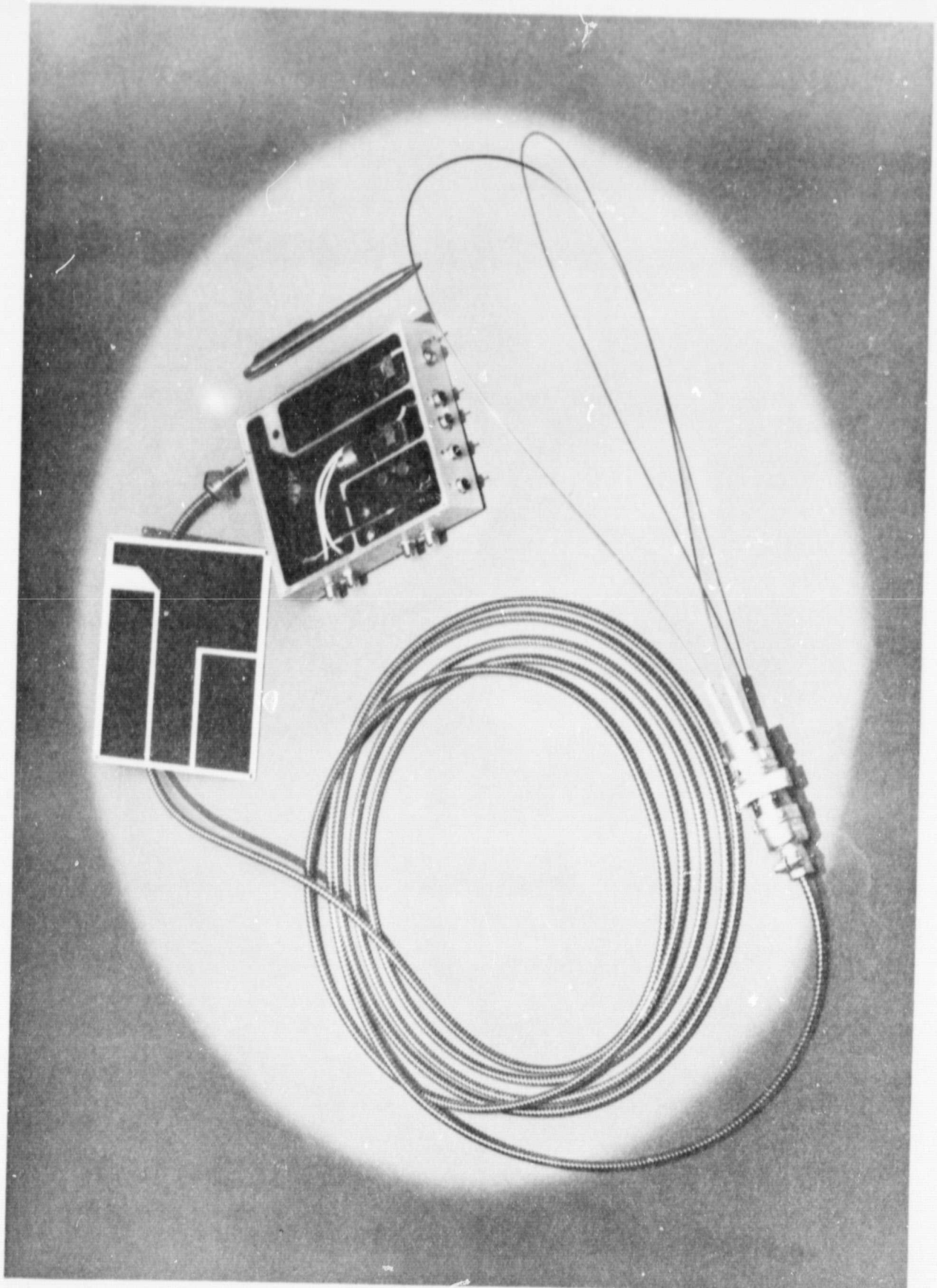
In order to build the optics module and sensor head, we had to learn, often through trial and error, how to make fusion splices, four-port couplers, fiber connectors, and to effectively couple the fibers to epoxy encapsulated LED light sources. Difficulties were encountered several times with unprotected fibers breaking that were placed under a bending stress at rigid epoxy joints. Making the epoxy joints to the fiber buffer coating eliminated this problem. In one instance, the temperature sensor head was accidentally operated above the rated temperature and one LED was damaged by running at average current levels above the rated maximum. As a consequence, the optics module and sensor head had to be rebuilt with new components to bring the signal levels back to a level of good detectability. The rebuilt module and sensor head gave improved signal levels with better splices and a smaller connector loss.

Figure 3-1 shows a photograph of the optics module and sensor head. The sensor head consists of a two fiber connector and a temperature sensing loop. The sensor head is connected to the optics module with a 15 ft length of flexible metal conduit that contains the two fibers from the sensor loop. The optics module is shown with the lid removed and contains the LED's, LED modulators, the four-port coupler, the reference and sensor leg detectors, focusing optics, and optical filters required to separate the two wavelengths. Details of the construction and mechanical layout of the optics module will be discussed in the next section. In Section 3.3 we will discuss the construction and design of the optical components; and in the subsequent section, we will discuss the electrical circuit, including the LED modulators and detector electronics. We will also discuss the timing sequence for the modulators and signal processing electronics; and calculations will be presented for the signal-to-noise ratio and minimum detectable temperature.
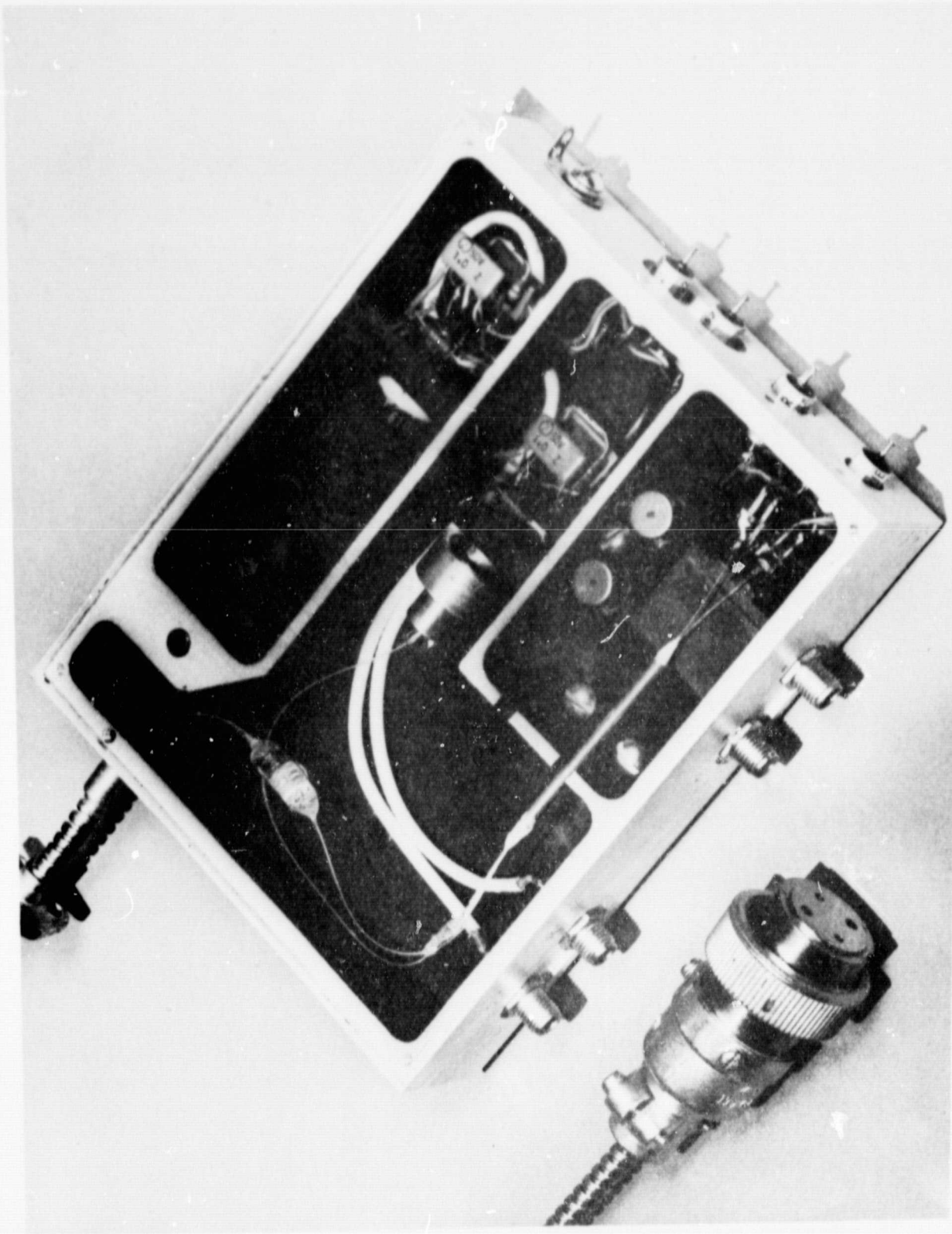
3.2 Mechanical Layout

Figure 3-2 shows a close-up view of the optics module and the two fiber connector which is disengaged from the sensor head. The various components in the optics module are labeled in the following illustration, Fig. 3-3. The module consists of a 4 in. x 5 in. x 1 in. aluminum box with a recessed lid for shielding against electromagnetic and optical interference. The inside of the box is compartmented and painted black to eliminate any possible optical or electrical crosstalk between the reference and sensor detectors.
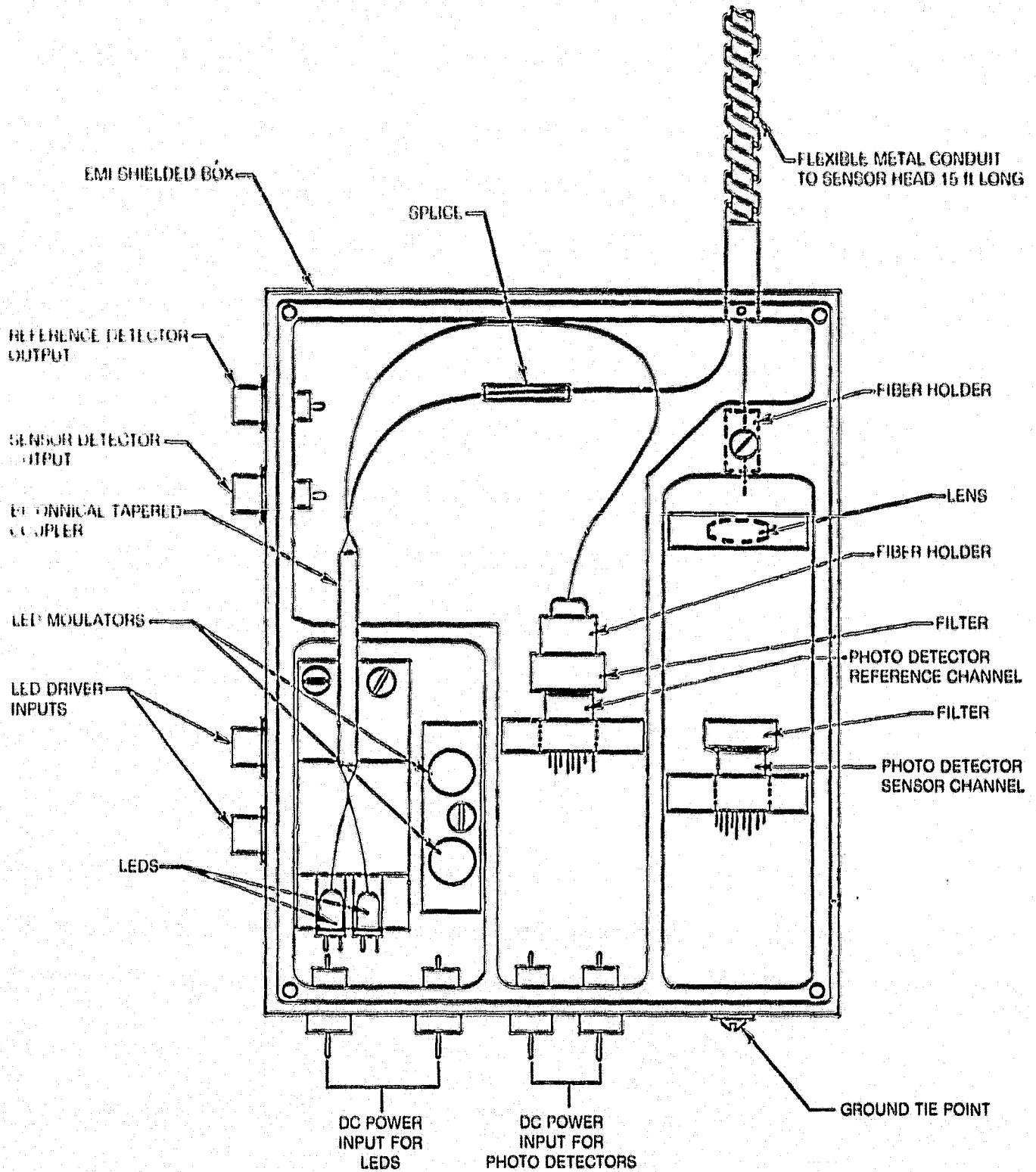
OPTICS MODULE AND SENSOR HEAD

80—2—49—1

FIG. 3.2

CLOSE-UP OF OPTICS MODULE

FIG. 3 3

MECHANICAL LAYOUT OF OPTICS MODULE

EMI SHIELDED BOX

SPLICE

FLEXIBLE METAL CONDUIT
TO SENSOR HEAD 15 ft LONG

REFERENCE DETECTOR
OUTPUT

FIBER HOLDER

SENSOR DETECTOR
OUTPUT

LENS

BI CONNICAL TAPERED
COUPLER

FIBER HOLDER

LED MODULATORS

FILTER

PHOTO DETECTOR
REFERENCE CHANNEL

LED DRIVER
INPUTS

FILTER

PHOTO DETECTOR
SENSOR CHANNEL

LEDS

DC POWER
INPUT FOR
LEDS

DC POWER
INPUT FOR
PHOTO DETECTORS

GROUND TIE POINT

80-G-72-10

17

The compartment in the lower left of the module contains the two LED's and their semiconductor FET modulators that turn the LED's on and off in accordance with the LED modulator input pulse rate. The fibers that collect light from the LED's are joined in the four port coupler that is encased in the long thin tube. A plastic board supports the LED's and coupler. The tube holding the coupler extends out of the LED compartment as shown in the photo. The two fibers at the output end of the coupler have a component of light from each LED. One of the fibers bends into a fiber holder and illuminates the reference detector through a special order filter. The second fiber is spliced into a lead that connects with the sensor head through the flexible metal conduit. The return fiber lead from the sensor is terminated at a capillary tube fiber holder shown in the upper right corner of Fig. 3-3. Light emitted from the end of the return fiber is imaged on to the sensor channel photodetector through an optical fiber that has the same characteristics as the filter in the reference channel. By releasing a set screw the position of the return fiber holder can be adjusted along the axis of the lens. The lens is mounted into a plastic holder that is held to the bottom of the module box in an oversized hole with a screw and washer. A small adjustment of the lens position can be made by loosening the mounting screw, moving the lens holder and retightening the screw. The small adjustment in lens position was required since the sensing area of the photodetector is not concentric with the axis of the photodetector mounting can. Four SMA coaxial connectors on the right hand side of the module were used for the detector outputs and the LED modulator inputs as indicated in the illustration. On the lower side of the module are four electrical feedthrough bushings and a ground tie point that provide terminals for the DC power to run the LED's and photodetectors.

The sensor head consists of a double fiber connector and a 30 cm long loop of 50 mil diameter stainless steel hypo-tubing that contains the europium doped, temperature sensitive section of fiber. The connector was made from the shell of a Cannon WK-4-22C and WK-4-31S four pin electrical connector. Two alignment pins on the connector body and a groove on the shell give a precise alignment and orientation to the two parts of the connector upon mating. The fiber diameter was 9.5 mils. To drill two holes with a diameter that small in mating parts is a fairly difficult task. Instead, larger recessed holes were drilled that precisely fit a sapphire jewel. The sapphire jewel had a precision hole that nearly fits the fiber diameter.

The hypo-tubing loop that supports and protects the sensing fiber terminates at the connector in two ceramic tubes as shown in Fig. 3-1. The ceramic tubes give thermal insulation between the hot sensing fiber and the connector and keep the connector temperature not too far above room temperature when the sensing loop is placed in an oven.

The four fibers, two for each half of the connector, were threaded through the sapphire jewels and potted in place with a hard epoxy. The ends of the connectors

connectors were then ground and polished on a lap to produce a good optical finish
on the ends of the fibers. Unfortunately, one of the fibers had been tilted off
center and ended up with about one third of the core diameter of misalignment. A
misalignment of this amount would give an additional loss of about 2 to 3 dB for
the connector. Since it is difficult to correct alignment problems with the com-
pleted connector, we decided to live with the additional loss for the present program.
Later in the program, as previously mentioned, the sensing loop was overheated to
temperatures well above 500°C and the transmission of the sensor head decreased to
20 percent of its original value. A new fiber connector and sensing loop was made.
Due to time limitations, a less complicated connector was made that uses splices
and could be rebuilt without much difficulty if the sensing loop were overheated
again.

3.3 Optical Circuit

3.3.1 LED Emission and Coupling to a Fiber

A general schematic of the optical circuit for the optics module and sensor
head is shown in Fig. 3-4. This figure illustrates the optical and fiber otpical
component layout that was discussed in the previous section. Galite-type 3000 LC,
204 µm diameter core fiber with a PVC buffer coating was used throughout the
optics circuit except for the europium sensing section of fiber that we produced
ourselves. The operation and construction of the different components of the optical
system will be discussed in this section.

The longest wavelength that gave a temperature dependent absorption in the
europium fiber was 610 nm. We tested different types of visible LED's from Texas
Instruments, Opcoa, and Monsanto (now General Instrument Optoelectronics) in the
610 nm wavelength range to determine the best LED to use. All the visible LED's
are encapsulated in epoxy and sold on the market as indicator lights. The prices
for the LED's range around 50 cents. Visible LED's are constructed from gallium
arsenide phosphide, $GaAs_{(1-x)}P_x$. By varying the arsenide/phosphide ratio, the
central emission wavelength of the LED can be adjusted. With no arsenide the LED
emits at its shortest wavelength of 565 nm, and at the other extreme with no phosphide
at the LED emits at the longest wavelength of 940 nm. The radiated power per unit
area from the LED's is directly related to the emission wavelength, the long wave-
length LED's being considerably stronger radiators than the shorter wavelength LED's.
We chose the longest wavelength absorption in the europium fiber for this reason.

Spectral emission widths of the LED's are typically 40 nm. The absorption width
of the europium fiber, however, varies from 5 to 15 nm over the temperature range of
interest. In order to obtain the largest percentage change in the optical signal
with temperature we need a bandpass filter that passes only the light that is
affected by the absorption. There are no standard LED's made that have a central

FIG. 3.4

SCHEMATIC OF OPTICAL CIRCUIT FOR FIBER OPTICS TEMPERATURE SENSOR

80-0-72-0
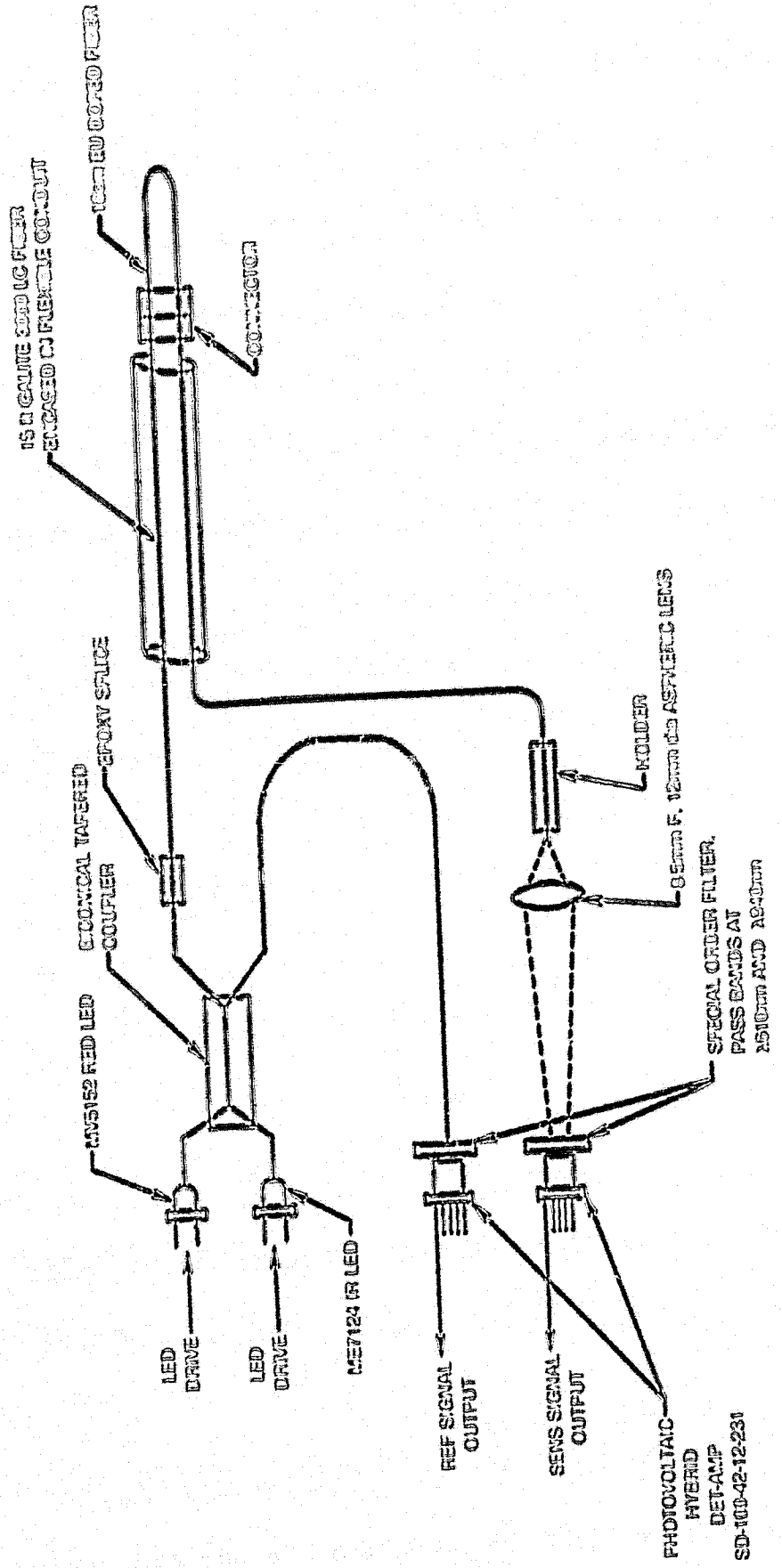
emission wavelength at 610 nm; however, it would be possible at much greater expense
to have an LED made at the correct emission wavelength. Of all the LED's tested, a
Monsanto MV5152 gave the greatest power through a 610 nm, 10 nm full width, half
maximum bandpass filter and was chosen for the temperature sensor. Figure 3-5 shows
the spectral power output of an MV5152 LED before and after filtering with the 610 nm
bandpass filter. Only five percent of the optical power from the LED is passed
by the filter.

The optical power emitted by a batch of the same type LED's can vary by as
much as a factor of 2. We selected the highest power MV5152 LED out of a dozen.
The best LED emitted an optical power of 60.6 μW, but only 0.7 percent or 424 nW could
be focused with a lens into a 200 μm core, 0.48 numerical aperture (NA) fiber. The
epoxy encapsulation around the top of the LED is spherical to form a lens. In
addition, there is a parabolic reflector behind the LED to help collect the side
emitting light and direct the light forward. But cutting the top of the LED lens
flat and drilling a small hole, we could place the end of the fiber near the LED
emitting surface. The fiber had to be aligned in the drill hole with an x, y, z
micrometer positioner to obtain the maximum coupling of optical power. The fiber is
then frozen in the position of maximum coupling by potting in a clear epoxy. We
found that it is important to have the epoxy potted to the buffer coating on the
fiber to help provide a strain relief for the fiber on bending. Coupling the fiber
to the LED in this manner (butt coupling) gave a surprising factor of five improve-
ment over lens coupling. Butt coupling is the most efficient coupling one can make
if the source is larger than the fiber core that collects the light and if the fiber
end can be placed against the emitting surface. In our case, however, we could not
place the fiber directly on the emitting surface without damaging the LED. By
making a small lens in the end of the fiber with an arc splicing device, we could
increase the light coupling another 20 to 50 percent. With the best coupling, then,
we obtained about 1.8 μW or 3 percent of the optical power from the LED into the
fiber. Losses of the optical filter at the detector, absorption by the fiber, and
losses in the coupler and splices reduce the power level to 29 nW by the time we
detect the signal at the sensor photodetector. A Monsanto ME7124 was chosen as the
source to produce a wavelength separated from the temperature dependent absorption.
The peak emission wavelength of the ME7124 LED is 940 nm. This IR LED is considerably
more powerful than the ME5152 red emitting LED.

The optical power and spectrum emitted by an LED are functions of the tempera-
ture of the semiconductor junction (Ref. 2). Radiated output power, from the LED's
can typically decrease by 1 percent per degree centigrade, and the peak wavelength
of the radiated output increases by 0.09 nm per degree centigrade for indirect band
bap materials and 0.2 nm for direct band gap materials. The spectral shift of the
MV5152 LEd would lie somewhere between these two values. To obtain a maximum signal
level, the MV5152 LED is operated at its maximum rated average current of 35 mA. As
a consequence, the junction temperature rises above ambient after turn-on and
reaches a steady state value after a sufficient length of time when thermal equilibrium

FIG. 3.9

SPECTRAL POWER FROM RED LED SOURCE WITH AND WITHOUT FILTER

80-0-72-8
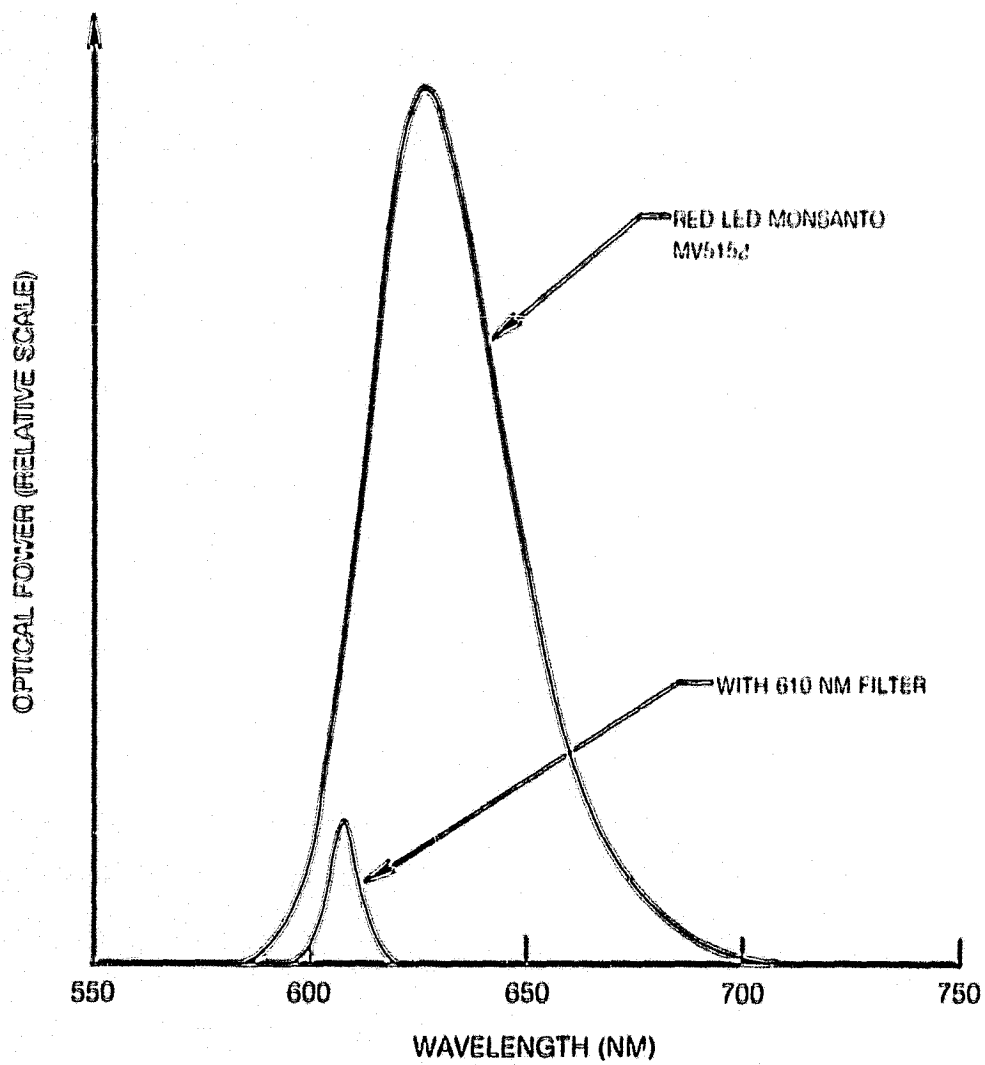
is established. We found that the detected signal from the MV5152 LED decreased to 79 percent of its initial value at turn-on with a characteristic (1/e) decay time of 25 sec. The ME7214 infrared LED, however, has excess power at its maximum rated average current of 100 mA and is operated at only 3.2 mA for the temperature sensor. As a consequence of the low drive current, the ME7124 LED gave no measured (< 5 percent) decrease in the optical signal level after turn-on. The spectral shift of the LED's may represent a problem with the temperature measurement and for a given accuracy set a limit over what range of temperatures the optics module can operate. In addition, the central wavelength of the interference filters can shift 0.03 nm per degree centigrade to longer wavelengths. The spectral shift and its possible effect on the temperature sensor will be discussed in a later section.

3.3.2 Four Port Coupler

To make the temperature sensor independent of signal amplitude and measure the transmission of the sensing fiber vs temperature, the emission from both LED's has to be placed in the same fiber. In addition, a fraction of the two sensor input signals must be sent to a reference detector to normalize the inputs and make them insensitive to source intensity changes. A four port fiber optic coupler solves this problem by mixing two input channels and giving outputs for the sensor and reference channel that contain both inputs at some fixed ratio.

We constructed two types of four port couplers. The first coupler used a section of rectangular core fiber that had two input fibers butt coupled to one end and two output fibers coupled to the opposite end. The optical power from each input fiber is split equally at the two output fibers if the coupler is made long enough. A cross section photo of the rectangular core fiber and an illustration depicting the coupling of input and output fibers is shown in Fig. 3-6. Ideally, to obtain the best coupling, we want the least overlap loss. In this case the height of the rectangular fiber core should just equal the input and output fiber core diameter, and the width of the rectangular core should equal two fiber core diameters plus two cladding thicknesses. The ideal excess coupler loss would then be:

$$L_c = 10 \text{ Log } [d / (d+dt)],$$

where d is the core diameter of the input/output fibers and t is the cladding thickness. For Galite 3000 L_c fibers the excess loss in addition to the 3 dB splitting ratio is 1.5 dB.

In addition to the area match, the coupler length has to be long enough to mix the two inputs. We chose a length of about 100 fiber core diameters (2 cm) that should allow enough mixing. If the NA of the rectangular coupler fiber is less than the NA of the input/output fibers, then not all the light will be captured by the coupler at the input; and if the NA of the coupler is greater than the NA of

23

FIG. 3.6

RECTANGULAR CORE FIBER FOR TRANSMISSIVE 4-PORT STAR COUPLER
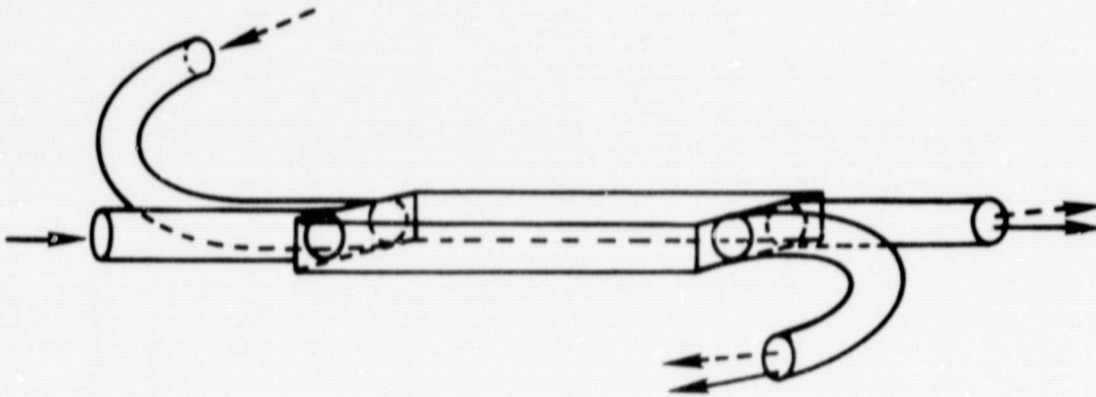
ORIGINAL PAGE IS
OF POOR QUALITY
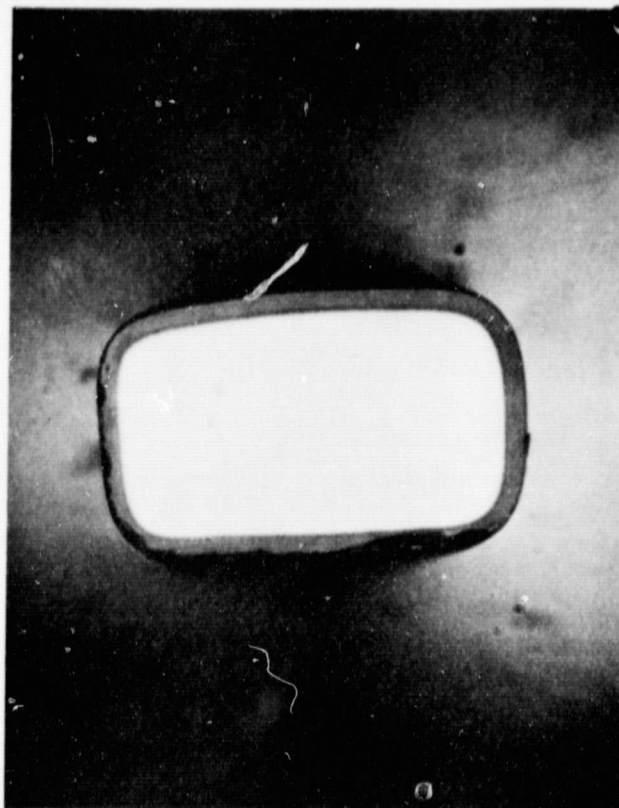
100 μm

fibers, then some of the light at the output end may not be collected, although the latter case is more desirable since the input optical rays will maintain their emitted angles to a certain extent. Several rectangular core couplers were made, and the best coupler had an excess loss of 3 dB.
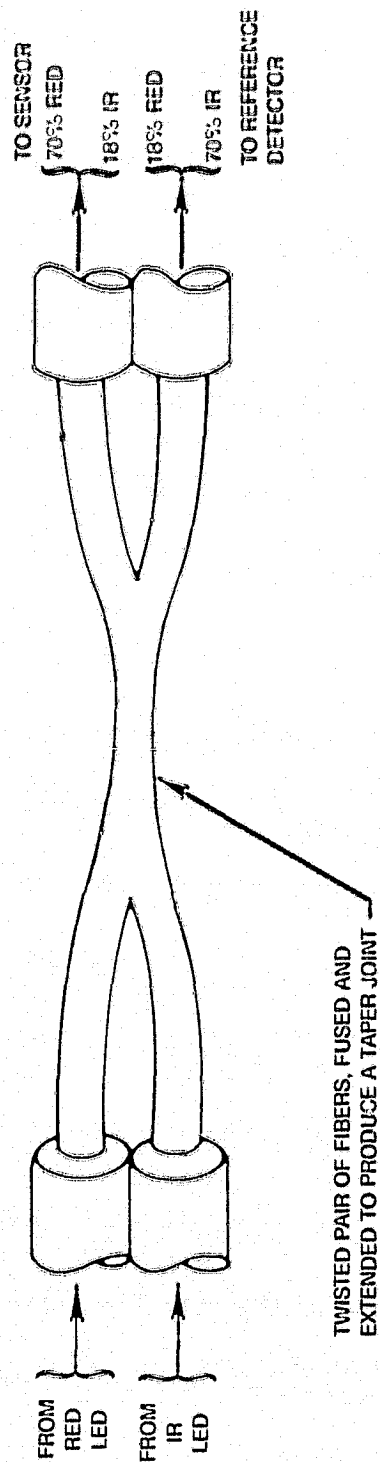
Most of the coupler effort was made on the biconical tapered coupler of Kawasaki and Hill (Ref.. 3). The coupler is depicted in Fig. 3-7 and is constructed by twisting a pair of fibers under slight tension, fusing the twisted joint with a torch or small heater wire furnace, while at the same time extending the fusing joint to produce a taper with a central diameter about the same size as one fiber. The coupling ratio and excess loss was monitored at intervals in the process by detecting light transferred from one input fiber to the two output fibers. After making many couplers, we found that it was important to keep a smooth taper at the coupling joing to avoid a large excess loss. The excess loss in this case occurs mainly by not recapturing all the cladding light in the fiber core on expansion back to the original fiber size at the output. The light retained in the cladding is stripped off into the buffer coating within a short distance.

Making the couplers with a torch gave inconsistent results and was hard to control. To help eliminate the inconsistances, we built a small Kanthal wire furnace. The furnace surrounded the fiber, but had a slot in the top portion so the twisted pair of fibers could be lowered into the furnace. A slight taper was built on the furnace to make the central region the hottest section. Several tapered couplers were made and excess losses varied from 1.8 dB to 0.5 dB depending on the smoothness of the taper and the coupling ratio. In general the smaller the fraction of optical power coupled the smaller was the excess loss. The fraction of power coupled increased as the taper was made smaller. We were interested in coupling of 20 to 35 percent; this range of coupling was relatively easy to produce. Figure 3-5 shows the coupling ratios from the two LED's for the coupler used on the temperature sensor. For this coupler, 70 percent of the Red LED power went to the sensor channel and 18 percent to the reference channel. The other 12 percent was lost in the cladding. For the ir emitting LED, the ratios were just reversed, as might be expected.
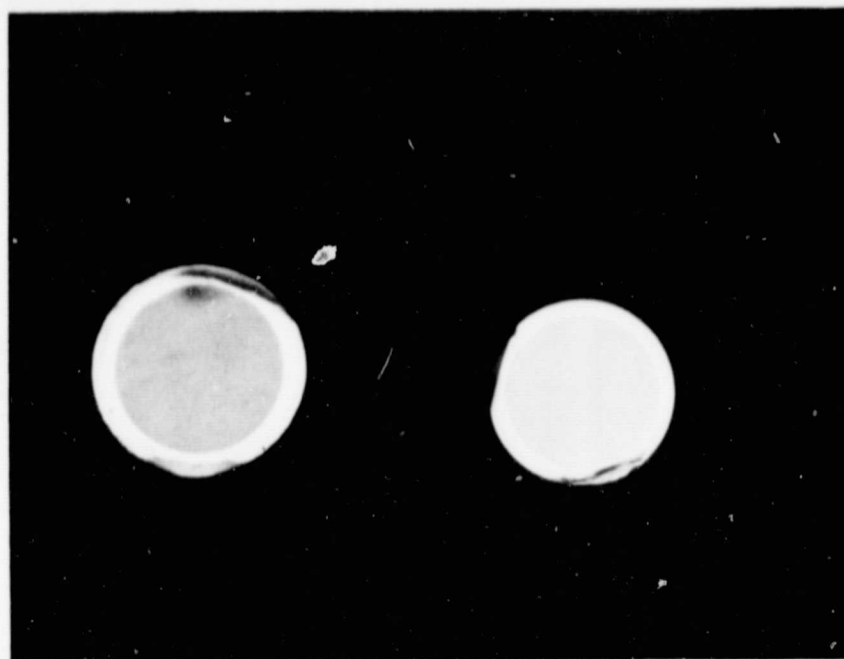
3.3.3 Sensor Fiber

The temperature sensing fiber was made from a high expansion borosilicate glass that was doped with europium to a 15 percent concentration. The special glass was purchased from an outside vendor in cane (i.e., rod) form. We used Kimble-type EN1 glass tubing for a cladding glass and pulled several spools of sensing fiber from the rod and tube, with the fiber pulling apparatus constructed at the Research Center. Figure 3-8 shows a photomicrograph, enlarged 100 times, of the cross section of the temperature sensing europium fiber and the Galite 3000LC fiber. The europium fiber core would give a red emission from the end of the fiber when the spool of fiber was illuminated with room lighting. The red glow was from trapped fluorescence of the europium ion in the fiber core.

FIG. 3.7

BICONNICAL TAPERED COUPLER

FROM
RED
LED

FROM
IR
LED

TWISTED PAIR OF FIBERS, FUSED AND
EXTENDED TO PRODUCE A TAPER JOINT

TO SENSOR
70% RED
18% IR
18% RED
70% IR
TO REFERENCE
DETECTOR

80—6—72—7

26

FIG. 3.8

FIBER CROSS SECTIONS

EUROPIUM DOPED
FIBER

GALITE 3000 LC
FIBER

FIG. 3.9

TEMPERATURE SENSING FIBER

FUSION JOINT

GALITE 3000LC

ENI GLASS CLAD,
EUROPIUM GLASS CORE

GALITE 3000LC
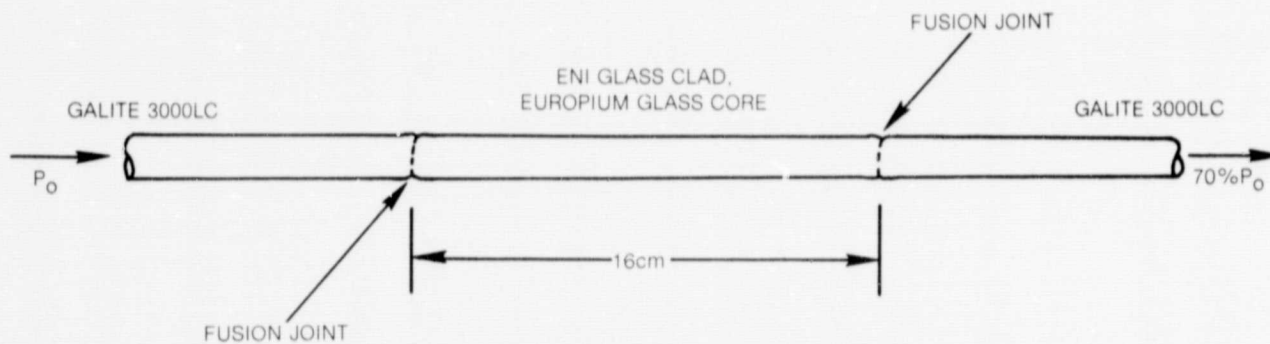
P_0

70%P_0

16cm

FUSION JOINT

80-6-72-5

Figure 3.9 illustrates the construction of the sensing fiber. Two pieces of Galite 3000LC fiber were fused to a 16 cm long section of the europium fiber with a fiber fusion apparatus, also constructed at the Research Center. In general, there is little or no difficulty in fusing cleaved or polished ends of identical fibers. The transmission loss through a fusion splice of identical fibers is less than the Fresnel reflection loss of the fiber joint before fusion. When the fibers are dissimilar, though, additional scattering losses can be generated at the fusion joint. In dissimilar fiber splices, the melting points and expansion coefficient of the glasses can differ. Bubbles and scattering surfaces can develop at the interface of the splice and cause the additional losses by scattering a fraction of the optical signal from the fiber core.

Several sensing fiber sections were made as shown in Fig. 3-9 for the hypotubing loop discussed earlier. Transmission losses at unabsorbed wavelengths ranged from 5 dB to 1.5 dB. The NA of the europium fiber is 0.44 and of the Galite fiber is 0.48. As a consequence, not all of the incoming optical signal from the Galite will be captured by the europium fiber. The loss due to the NA mismatch goes as the square of the NA ratio and calculates to be 0.7 dB. The cross section of the fiber cores was made to overlap by choosing a slightly tapered section of europium fiber that had a core slightly larger than the input fiber and slightly smaller than the output fiber. If we allow for the NA mismatch loss, the excess scattering loss for the two fusion splices in the best sensing fiber was only 0.8 dB.

3.4 Electrical Circuit

3.4.1 General Description

The electrical circuit for the optics module is straightforward and shown in the schematic of Fig. 3-10. Two Semiconductor Products' 15 V power supplies are used to drive the module. One supply is split into two branches to power the two LED optical sources. Each branch has a helipot to set the average LED current. A shunt resistor is used in each branch to measure the current. The LED's are modulated with Type 2N6659 MOS FETs placed in series in the cathode lead of the LED. An 8 V Zener diode protects the FET from overdriving with the modulator input signal.

The photodetectors were Silicon Detector Corporation (SDC) Type SD-100-42-12-231 hybrid detector-amplifier. The diodes were blue enhanced and principally designed to operate in the photovoltaic mode, that is, with no reverse bias. In applications where high bandwidth is not required, the photovoltaic mode has an advantage of having no dark current from reverse biasing. This feature improves the signal-to-noise (S/N) ratio and gives the detectors a lower noise equivalent power. The internal capacitance in the photovoltaic mode, however, is greater than in the photoconductive or reversal bias mode; and consequently, the photovoltaic mode has a lower bandwidth. Bandwidth limitation can be a potential problem with time domain multiplexing and will be discussed later.

FIG. 3.10

SCHEMATIC OF ELECTRICAL CIRCUIT FOR OPTICS MODULE

80—6—72—4
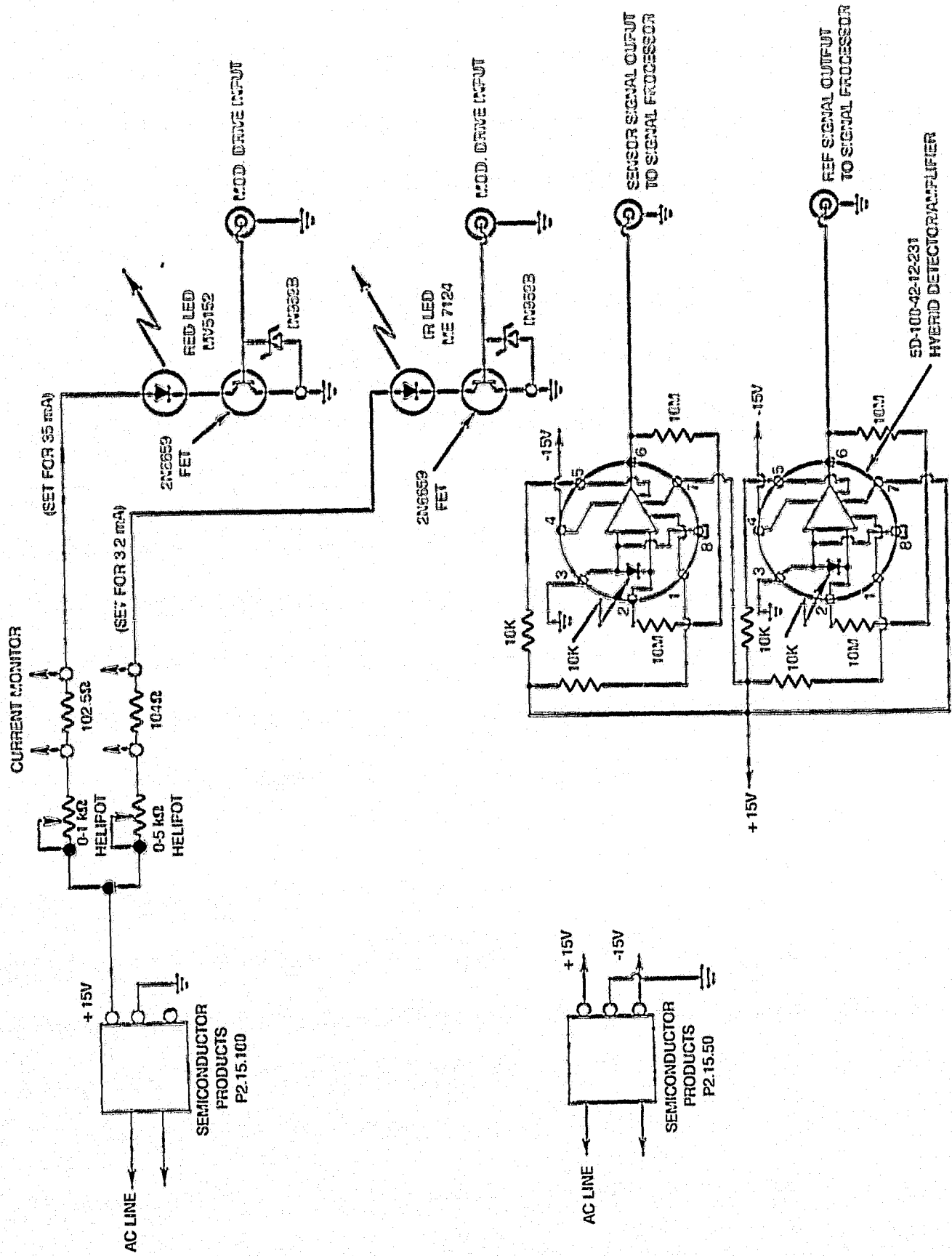
3.4.2 Detector Output and Timing Sequence

The photodetector has a response of 0.38 amps per watt of incident optical power at λ 610 nm. With the 20 MΩ feedback resistor used with the amplifier, the output signal is 7.6 mV per nanowatt of incident optical power. At λ 940 nm the responsivity of the photodetector is 0.41 A/W and the output potential is 8.2 mV per nanowatt of incident power. Figures 3-11 and 3-12 give the output signals from the sensor channel and reference channel detectors with the sensor probe and room temperature. The 5 msec pulse output signals from both LED's are shown independently. The red LED is driven at its maximum average current and the output signal decays slightly during the driving pulse. There is no decay with the ir LED signal. We found that running the red LED with shorter pulses but at the same average current caused an even greater drop in the red signal during the driving pulse. This effect may be due to the complete utilization of the change carriers in the semiconductor junction of the LED. The pulse rate was 100 Hz for the red LED and 50 Hz for the ir LED. The reasons for the different pulse rates will be described later.

The detector output pulses shown in Figs. 3-11 and 3-12 were taken at room temperature, 23°C. When the sensing loop is placed in an oven and heated, the red LED signal decreases in magnitude. Figure 3-13 shows a plot of the ratio:

$$f(T) = [V_S(red)/V_S(ir)][V_R(ir)/V_R(red)]$$

where $V_S(red)$ and $V_R(red)$ are red emitting LED signals in the sensor and reference channels. The signal levels were taken from oscilloscope traces and could be read to about 5 percent accuracy. The data was normalized to 1.0 at the 0°C measurement. The data points approximately fit an empirical function:

$$f(T) = e^{-T/566} .$$

The exponential fit may be coincidental, since there is no obvious theoretical reason why the temperature dependence need be exponential in this case.

The output of the detectors go to a signal processing unit to be discussed in more detail in the next section. In the signal processing unit, each pulse from the photodetector is integrated and then a sample-hold circuit reads the result of the integration. The held signal level is then converted to a digital output through an A-to-D converter. The integration, hold, and conversion is done sequentially every 5 msec so that both wavelength signals are read independently. In order to obtain the true signal level, we must also measure the dc level output of the detector with no light signal, and then subtract the dc level from the light signal level. AC coupling from the photodetectors would eliminate the dc level signal; however, in this case we would be taking the difference between the signals at the two wavelengths. To eliminate amplitude or power change error in the fiber as discussed earlier, we need to take a ratio of the signals at the two wavelengths.

FIG. 3.11

SIGNAL OUTPUTS

SENSOR CHANNEL

100 mV/div
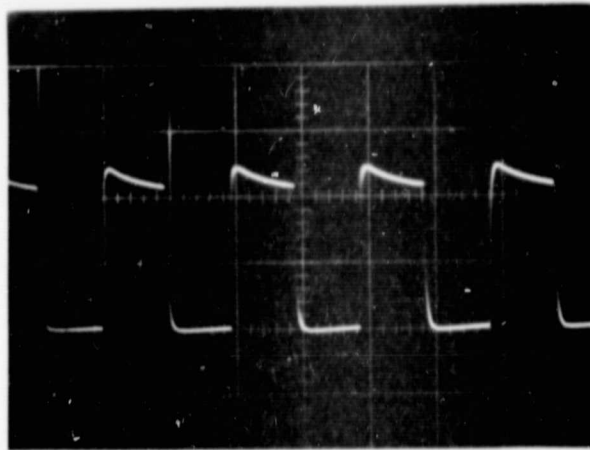
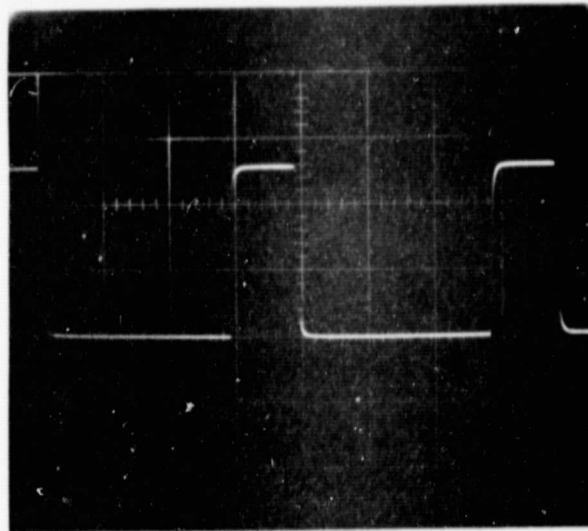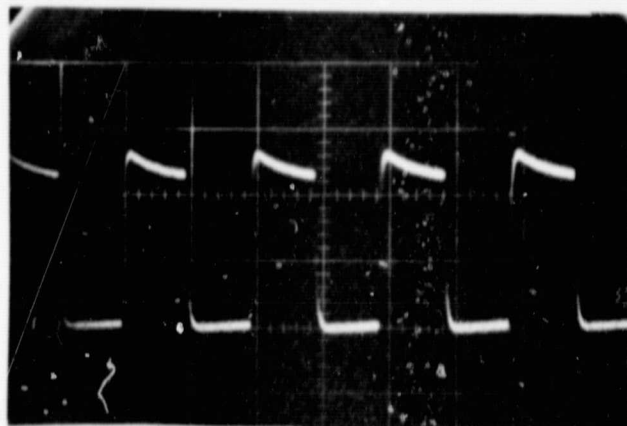RED WAVELENGTH

5 msec/div ⟶

50 mV/div

IR WAVELENGTH

5 msec/div ⟶

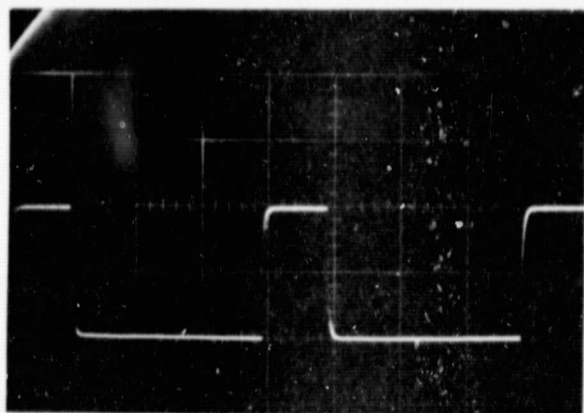80-6-72-3

SIGNAL OUTPUTS

REFERENCE CHANNEL

RED WAVELENGTH

20 mV/div

5 msec/div

IR WAVELENGTH

1.0 V/div

5 msec/div

TEMPERATURE DEPENDENCE OF EUROPIUM FIBER OPTIC TEMPERATURE SENSOR

SOLID CURVE $f(T) = \sigma^{-T/500}$

O DATA POINTS
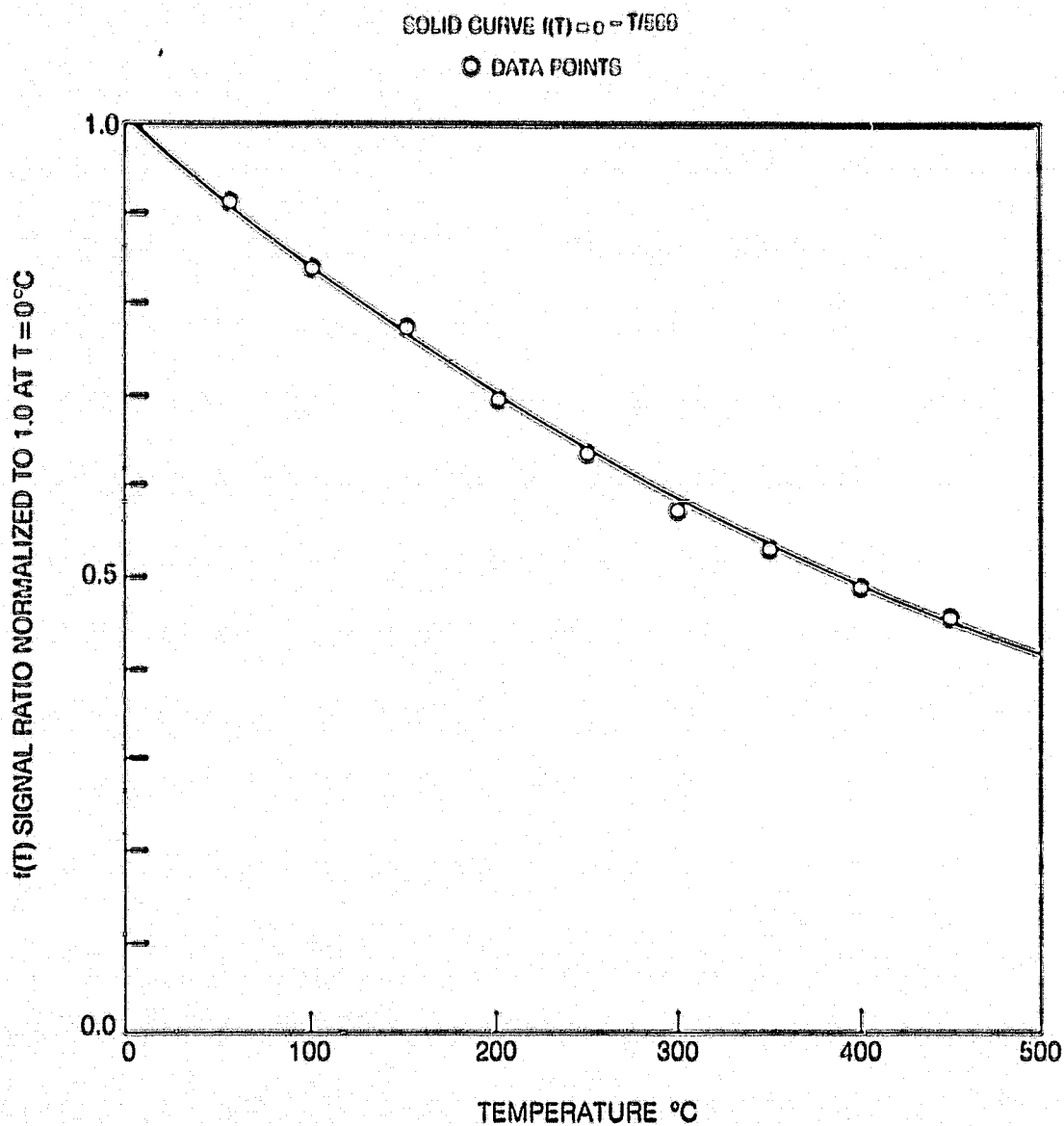
Reading the data from the two wavelengths sequentially (i.e., time domain multiplexing), requires that we also read the zero-light signal level from the detector and subtract to get the true signal level.

The timing sequence, which is derived from the computer, is shown in Fig. 3-14. The red LED is pulsed on for 5 msec every 10 msec, and the ir LED is pulsed on for 5 msec every 20 msec. The ir pulse occurs between two red pulses on every other pulse. In this manner we can read a zero-light level pulse every 20 msec or between every other red pulse. The photodetector output signal is illustrated by the third trace in Fig. 3-14. The fourth trace or bottom trace shows the sequence of events for the integrator circuits. At a time 2 msec into the 5 msec pulse interval, the processor initiates integration. The integration period runs for 3 msec. The integrated signal level is then held for the next msec so that an A-to-D conversion can be made. For the last msec, the signal level is reset to zero and the process reinitiated for the next 5 msec interval. The temperature dependent function is then taken from the ratio:

$$f(T) = \{[V_{0}(red)-V_{0}(0)]/[V_{0}(ir)-V_{0}(0)]\}\{[V_{R}(ir)-V_{R}(0)]/[V_{R}(red)-V_{R}(0)]\}$$

where $V_{0}(0)$ and $V_{R}(0)$ are the zero-light or baseline signal levels.

The temperature function is computed every 10 msec with a new measurement at the red wavelength in the sensor channel and reference channel. The zero-light signal level and the ir signal levels are read every 20 msec and the temperature function is updated every 20 msec with these numbers. The last three parameters that are measured every 20 msec change only slowly in time in relation to the red wavelength signals so that the temperature response time is not sacrificed.
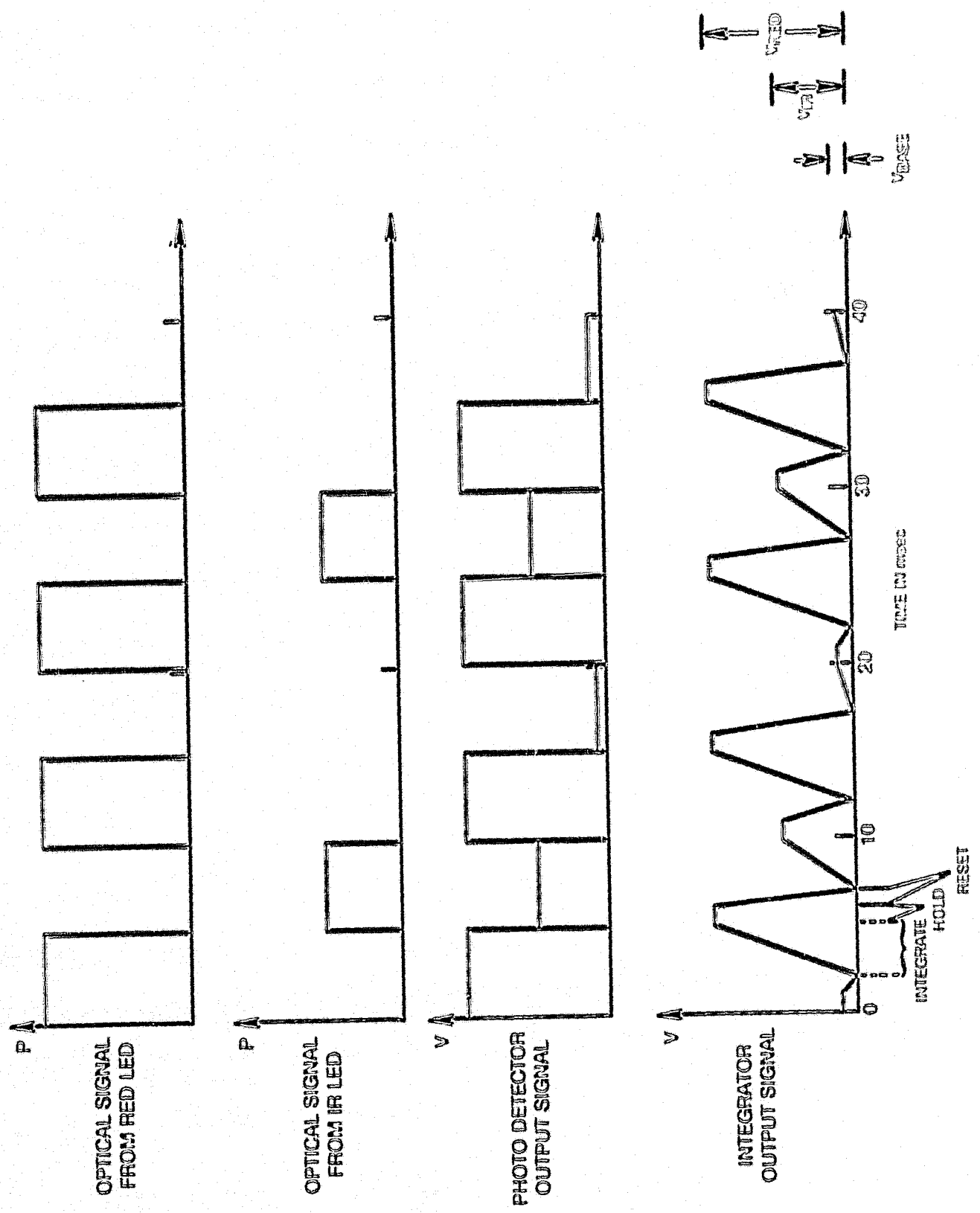
3.4.3 Signal-to-Noise and MDT

The noise level at the photodetector represents a fundamental limit on the sensitivity of the temperature sensor. We can define a minimum detectable temperature change (MDT) as that change in temperature at the sensor that produces a change in the photodetector signal just equal to the rms noise signal at the photodetector. The MDT is the very best sensitivity one could hope to achieve, since other effects such as power supply and amplifier variations or changes in the signal in one detector channel relative to the other channel can also give a temperature error.

The square of the rms noise current generated at the photodetector at a bandwidth Δf has three components (Ref. 4):

$$i^{2}_{n} = 4kT_{a} \, \Delta f/R_{s} + 2ei_{s} \, \Delta f + 2ei_{d}\Delta f.$$

FIG. 3.14

TIMING SEQUENCE FOR FIBER OPTIC TEMPERATURE SENSOR

OPTICAL SIGNAL FROM RED LED

OPTICAL SIGNAL FROM IR LED

PHOTO DETECTOR OUTPUT SIGNAL

INTEGRATOR OUTPUT SIGNAL

The first component is Johnson or thermal noise where R_f is the feedback resistor for the hybrid detector-amplifier and T_a the ambient temperature of the detector. The second component, where i_0 is the signal current, represents the quantum or shot noise, that is, the statistical noise when detecting discrete quanta. The last component is noise from the photodetector dark current, id, generated from a reverse bias potential. For the photovoltaic detectors used with the temperature sensor, the last component is zero since no reverse biasing potential is used.

The signal current is given by:

$$i_0 = RP_0 e^{-\gamma LT} ,$$

where R is the detector responsivity in amps per watt of incident optical power, and $P_0 \exp(-\gamma LT)$ is the incident optical power. The exponential factor allows for the temperature dependent absorption in the sensing fiber, where T is the sensing fiber temperature, L the sensing fiber length, and γ the absorption coefficient of the fiber, which depends on the concentration of europium ions in the glass.

The change in signal current with temperature, that is the temperature sensitivity, is given by:

$$di_0/dT = -\gamma L RP_0 e^{-\gamma LT} = (\alpha/T) RP_0 e^{-\alpha}$$

where $\alpha = \gamma LT$. We can determine the optimum length and/or concentration of fiber to use at a given temperature by setting the derivative of di_0/dT with respect to α equal to zero. Thus, at constant T:

$$\frac{d}{d\alpha} \left(\frac{di_0}{dT} \right) = \frac{RP_0 e^{-\alpha}}{T} \left(-1 + \alpha \right) = 0$$

and $\alpha = 1$. Therefore, for maximum temperature sensitivity, we want an absorption of 1/e in the sensing fiber. The 1/e absorption length or concentration should be chosen at a temperature that is in the middle of the temperature range to allow a good sensitivity over the entire range.

The signal-to-noise ratio at the detector would be given by:

$$S/N = i_0/i_n = RP_0 e^{-\gamma LT}/[4kT_a \Delta f/R_f + 2eRP_0 e^{-\gamma LT} \Delta f]^{1/2} .$$

The S/N in decibels is plotted in Fig. 3-15 vs the optical power P_0 in nanowatts. The parameters used were:

SIGNAL TO NOISE RATIO FOR TEMPERATURE SENSING FIBER AT 100Hz BANDWIDTH
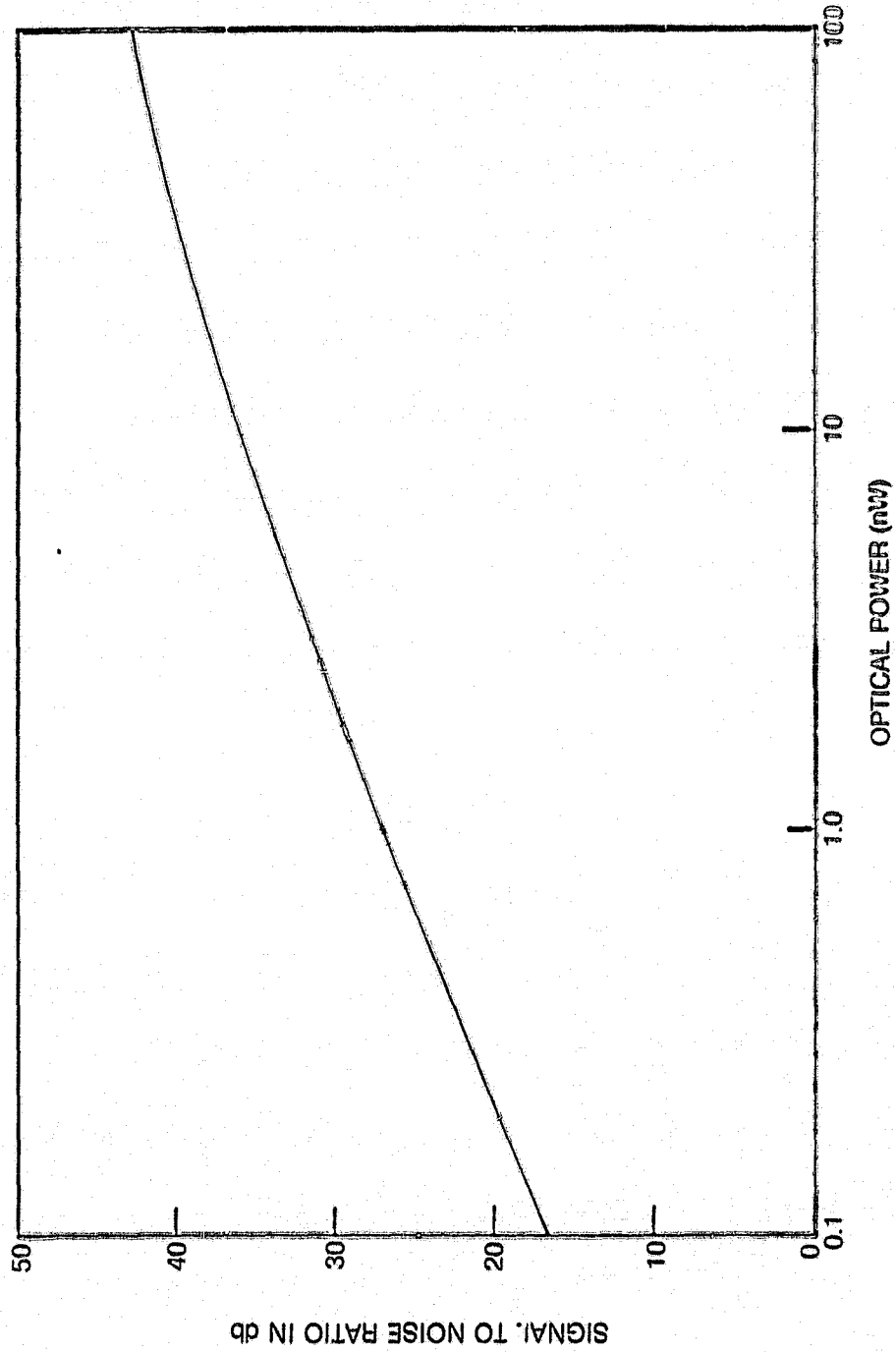
$$\gamma LT = 1$$
$$\Delta f = 100 \text{ Hz}$$
$$R_f = 20 \text{ m}\Omega$$
$$R = 0.35 \text{ A/W}$$

Signal-to-noise ratios greater than 30 dB should be achievable with optical signal levels of 5 nW. With a 100 Hz bandpass amplifier we measured noise current levels of 0.3 picoamps. The noise equivalent power or NEP of the photodetector would be given by:

$$NEP = i_n/R\sqrt{\Delta f} = 8.6 \times 10^{-14} \text{ W/}\sqrt{\text{Hz}}.$$

The NEP calculated from the Johnson noise is:

$$NEP = (4 \ kT_a/R_f)^{1/2}/R$$
$$= 8.2 \times 10^{-14} \text{W/}\sqrt{\text{Hz}}$$

and agrees within the measurement error of the measured NEP value.

A small change in temperature is related to a small change in signal current by:

$$\delta i_s = \gamma LRP_o e^{-\gamma LT} \delta T .$$

The minimum detectable temperature change, T_{min}, occurs when:

$$\delta i_s = i_n.$$

Therefore,

$$T_{min} = [(4 \ kT_a \Delta f/R_f) + 2eRP_o e^{-\gamma LT} \Delta f]^{1/2}/\gamma LRP_o e^{-\gamma LT} .$$

Using the previously mentioned parameters, we have plotted in Fig. 3-16 T_{min} vs. the absorption coefficient γLT for two optical power levels of 1 nW and 10 nW. A median temperature of 500° K was chosen for the calculation.

For the temperature sensor measurement we require four optical signals. The appropriate δT_{min} calculation in this case would have to allow for an accumulated noise from all the signals. The smallest optical signal, however, would be the greatest contributor of noise to the MDT. In our case the smallest signal was 4.5 nW at 500° K for the red emitting LED signal in the reference channel. Based on the photodetector noise alone, then, we should be able to detect temperature changes of about 1°C at midrange. There are other contributions to the temperature measurement error and they will be discussed later.

MINIMUM DETECTABLE TEMPERATURE CHANGE VS. ABSORPTION COEFFICIENT

Plot of δT in °C versus ABSORPTION COEFFICIENT (γ LT), with curves labeled $P_o = 1\text{nW}$ and $P_o = 10\text{nW}$.
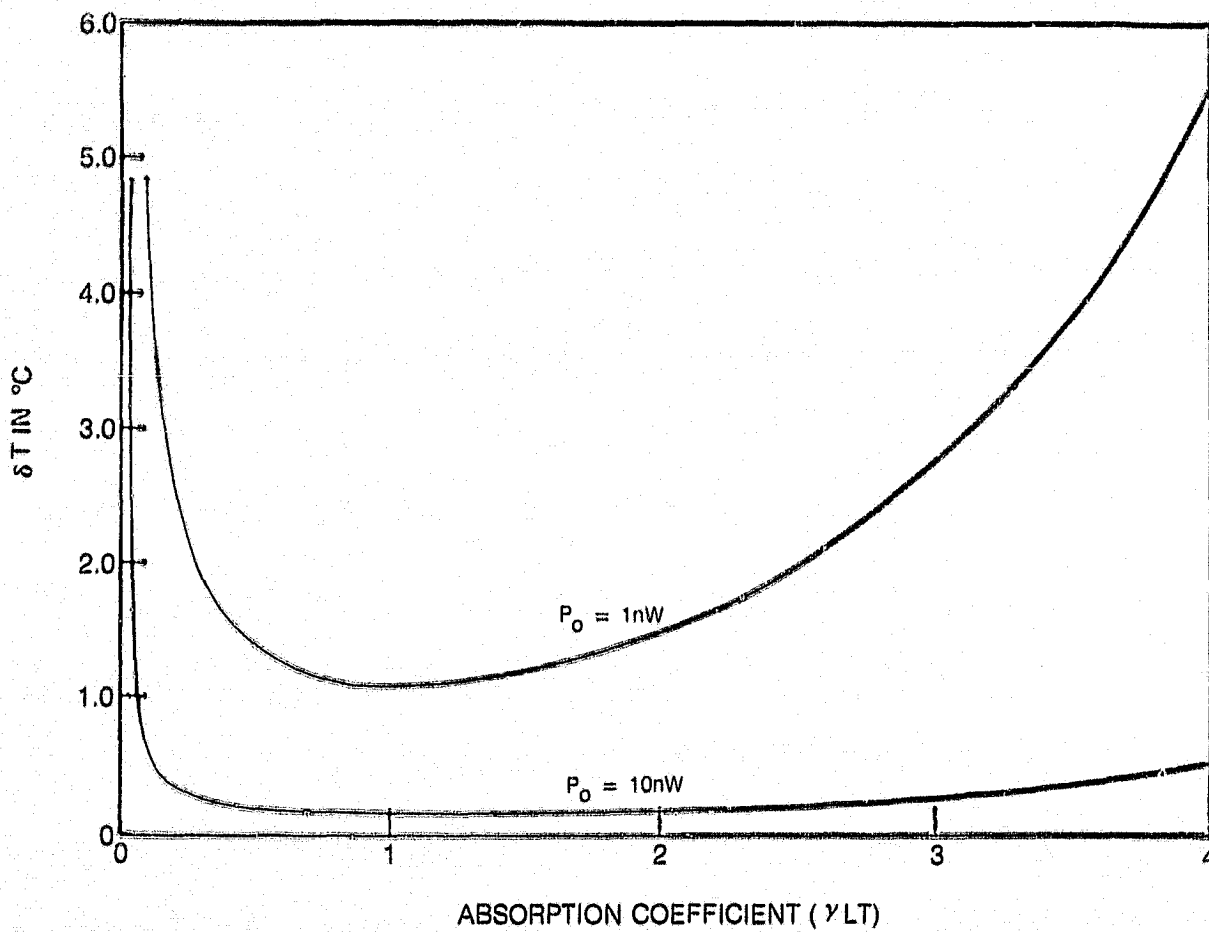
4. SIGNAL PROCESSING

The design of the optics module already described provides for a ratiometric approach to signal processing. This approach causes certain undesirable variables to be cancelled in the signal processing. The skeleton of this signal processing is to acquire a signal representing the transmission of light within a thermally dependent absorption band, and linearize and scale the result as temperature.

Processing is being performed digitally in order to attain a maximum degree of long-term stability. Analog components are subject to parameter variations coupled to age, temperature, and humidity. All but the absolutely necessary analog components have been eliminated, and the remaining analog parameters have been largely cancelled in the processing. A red LED provides a beam which is split into a thermally dependent signal path and a thermally independent reference path. Two detectors are employed to acquire the two signals which when ratioed eliminate LED intensity from the measure of red transmission. Difference in the gain of the two detector channels and detector gain changes are addressed by adding a second LED to emit IR radiation within a band not dependent on temperature. The two LED's are time multiplexed into the same optical system. Ratioing the two IR signals results in the IR transmission which is likewise insensitive to IR intensity. Ratioing the two transmissions produces a temperature dependent signal in which the analog gain of the two channels is also cancelled.

Each channel also incorporates an integrator to restrict bandwidth and thus improve signal-to-noise ratio. In order to cancel the effects of the background dc level from the photodetectors the integrator output with the LED's off is measured and subtracted from the signal and reference measurements.

Signals are acquired by a 12 bit analog to digital converter under the control of an 8-bit microcomputer. External hardware provides cycling of the LED's through a 4-count, 3-state sequence of RED, CAL, RED, IR. This sequence allows acquisition of the temperature dependent Red data each 10 ms period. The temperature independent IR and cal signals are updated alternately each 20 ms. The microcomputer provides synchronization with these states and acquires the data when the integrators are in the hold mode.

After acquiring the data, the microcomputer calculates the ratioing and scaling, then uses a lookup table to provide a linearized BCD output in degrees centigrade.

An Intel SYS80/204 microcomputer system was employed for the laboratory prototype in order to enjoy the benefits of mass production technology. Special custom processor configurations could be designed and fabricated for subsequent units if the volume or application warrant. The SYS80/204 was augmented with an SBC732 analog I/O board for signal acquisition and with an SBC310 board for high speed math processing. The SBC310 board provides 32-bit floating point calculation capability using Intel's 3000 series 2 bit bipolar slice technology.

40

Source program generation for this project was performed on a Tektronix 8002A Microprocessor Design Aid (MDA), purchased for the UTRC Microprocessor Development Center. This MDA also provides assembly, linking, simulation, and emulation.

Figure 4-1 shows a block diagram of the complete sensor. The portion in dashed lines is the optics module that is shown in more detail in Fig. 3-4. The system timing is controlled by an external oscillator and the CPU is slaved to it. This was done to allow preliminary testing of the optics module prior to completion of the software. In a next generation sensor the timing could be provided by the CPU, which would eliminate some external hardware and simplify the synchronization.

Figure 4-2 shows the run-time flow chart for the signal processing. The branching sequence is RED, IR, RED, CAL, as discussed. Each time RED data is acquired, the ratio is computed using previously acquired values for IR and CAL and an output is generated and sent to the display.

TEMPERATURE SENSOR BLOCK DIAGRAM

80—6—72—13

FIG. 4.2
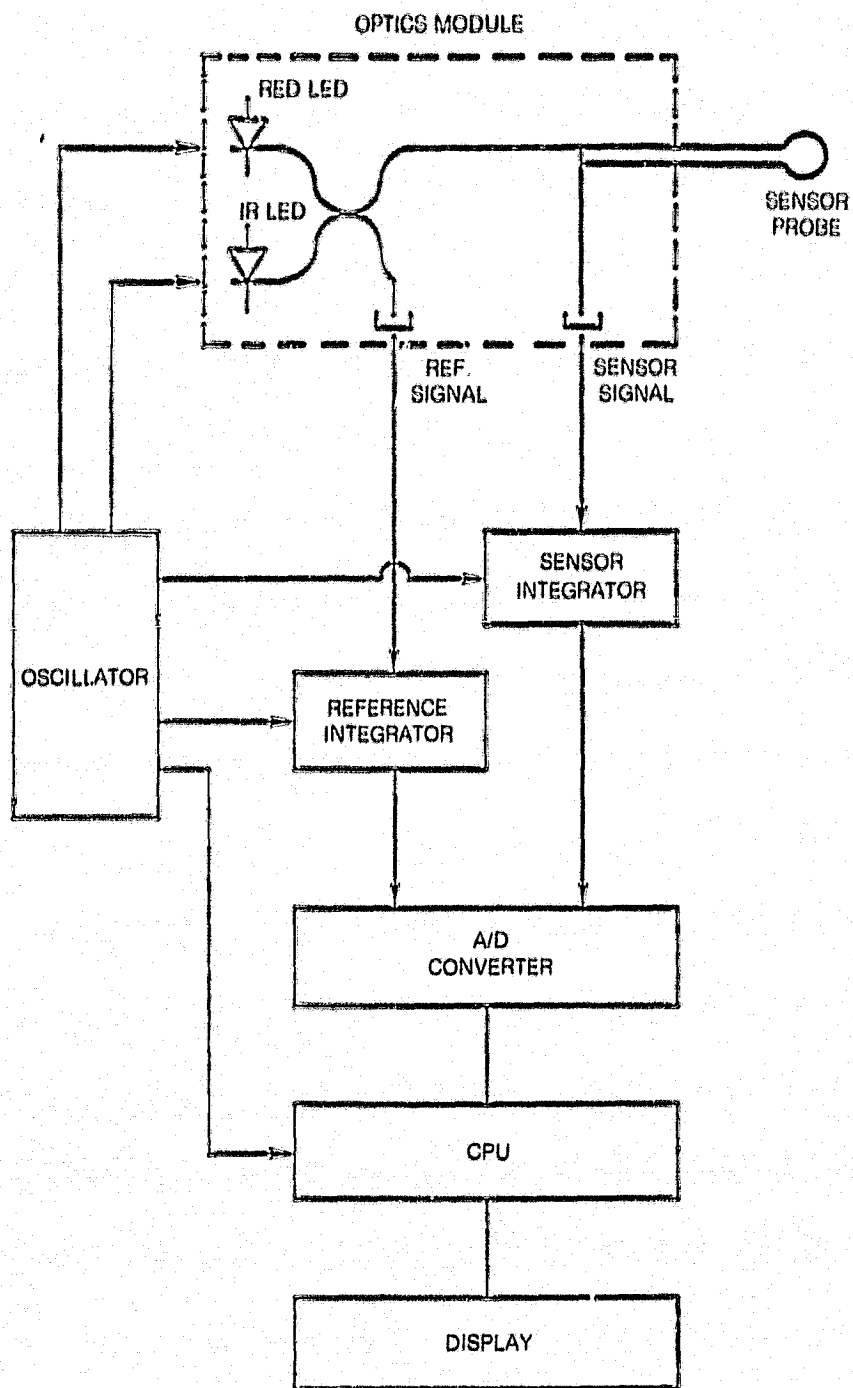
RUN TIME FLOW CHART
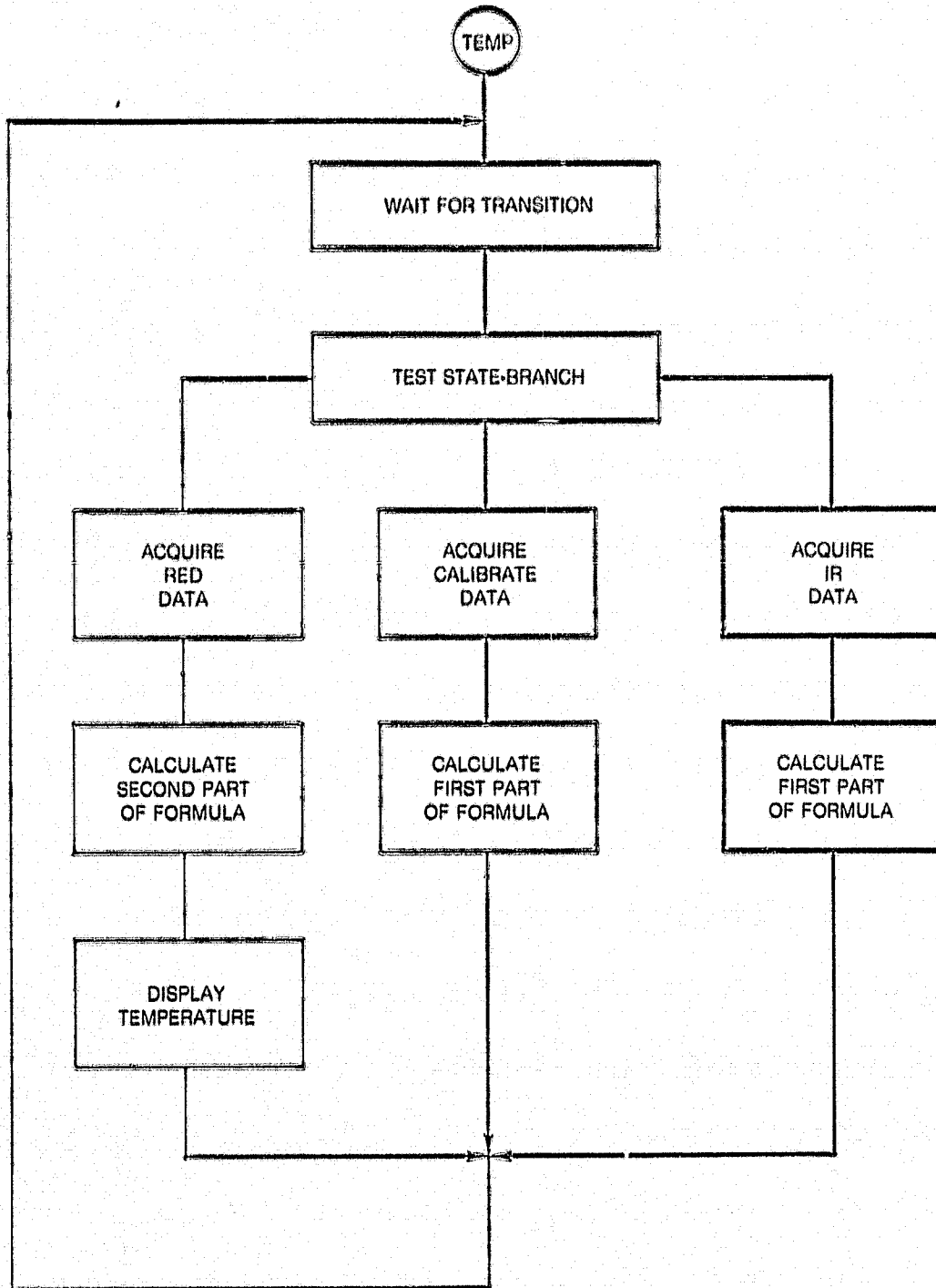
5. PERFORMANCE AND RECOMMENDATIONS

5.1 Sensor Operation

The operation of the sensor depends on the measurement of the probe transmission to a relatively high degree of precision. As discussed in Section 3, the normalized ratio follows the approximate empirical relation:

$$f(T) = e^{-T/T_0} \qquad (\ )$$

with $T_0 = 566°C$ (normalized so that $f(T) = 1$ at $T = 0°C$). The fractional change in this ratio is

$$\frac{df}{f} = \frac{1}{f} \frac{df}{dT} \ dt$$

$$\frac{df}{f} = \frac{1}{T_0} \ df$$

$$= 0.0017 \ dT,$$

or a change of 0.17 percent per degree centigrade. To achieve this accuracy requires extreme care in the signal processing even though the overall signal processing scheme is designed to cancel out most analog type error sources. The initial operation of the sensor revealed a number of problems. One problem was a slight A.C. ripple in the acquired data. Effects were made to minimize this by the elimination of ground loops in the signal processing and computing electronics; but it could not be completely eliminated. The effect of the AC line noise was to cause the least significant digit or degree in the output display to flicker rapidly at the 10 ms update rate. Some excess noise in the detector-amplifier hybrid circuits may also have contributed to this problem. To allow a stable display, a digital smoothing filter was incorporated into the processor. This was a Finite Impluse Reponse (FIR) filter that performed a 64 point running average on the data prior to display. This filter still provides an output at the 10 ms rate, although it reduces the overall effective system bandwidth.

With this modification, it was possible to obtain a stable output display of the transmission ratio. This ratio was measured at 25° intervals over the range of 0 to 400°C and a calibration curve was generated by a piecewise linear approximation. This curve is shown in Fig. 5-1. The vertical axis is the desired ratio of the transmissions at the two wavelengths. It has been scaled so that the range of possible values lies between 0 and 1023 ($2^{1-}-1$). The value of the scaled ratio is used as an address of a location in the memory. The content of the address is the corresponding value of the temperature in degrees centigrade.

FIG. 5-1

COMPUTER READOUT vs TEMPERATURE

COMPUTER OUTPUT IN SYSTEM UNITS

TEMPERATURE °C

80-G-72-14
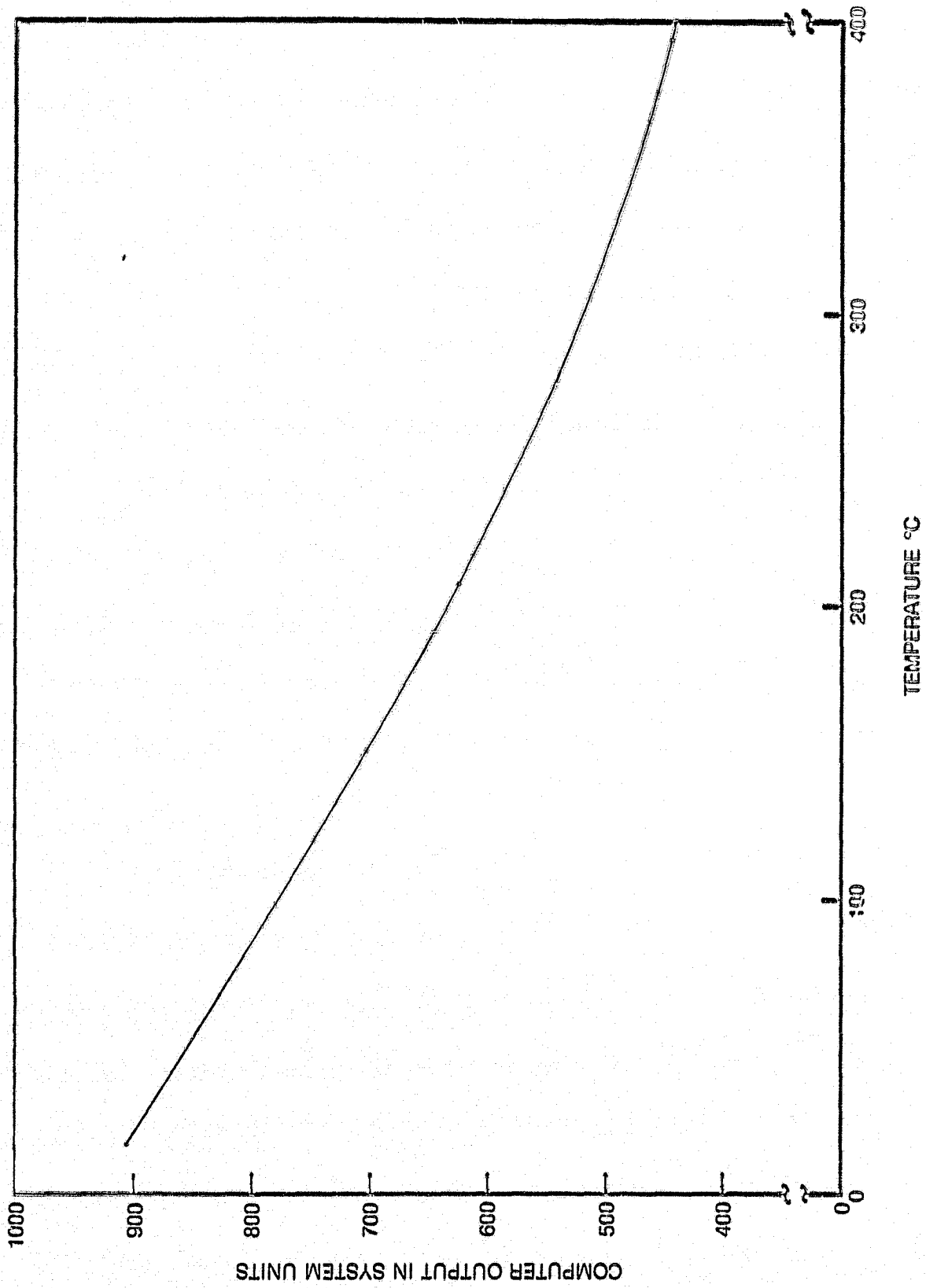
After an initial warmup period, the system output was observed to be constant to about $\pm$ 2 in system units at a constant room temperature. This corresponds to a fractional change in the ratio of $\pm$ 2/1000 or $\pm$ 0.2 percent. For a sensitivity of 0.17 percent/°C, this corresponds to a temperature stability of $\pm$ 1°C. At an absolute temperature of 293°K = 20°C, this is an accuracy of $\pm$ 0.3 percent of point which exceeds the 1 percent of point accuracy goal for the sensor.

There are, however, some additional problems that must be solved before this accuracy can be usefully realized in practice. The two major problems are a short term drift that occurs over a period of about five minutes after the LED's are turned on, and a long term drift which manifests itself in a change in the calibration curve over a period of several days. The magnitude of the short term drift is about 10-15 system units corresponding to 6-9°C. The magnitude of the long term drift is comparable.

The source of these drifts has not as yet been firmly established. A number of possible sources were considered including drift in the dc offset of the detector-amplifiers, cross talk arising from the time multiplexing of the RED, IR, CAL signals and changing characteristics of the LED's. At this time it appears that the problem of the short-term drift lies not in the electronic processor but in the LED/probe/filter/detector portion of the circuit. The signal processing scheme is designed to cancel out errors due to variations in the light intensity from the LED's and in fact, appears to do this. A potential problem, however, could arise if the spectrum of the RED LED changes as a result of temperature, drive level, or aging. As discussed in Section 3, the wavelength of peak emission of the RED LED does shift with temperature by an amount ranging from 2 nm to 4 nm (5 to 10 percent, cf. Ref. 2) during the initial warmup. The spectrum of the light actually transmitted through the probe to the detector is the product of the spectral transmission of the filter, the spectrum of the LED, and the absorption spectrum of the europium fiber sensor. Since the fiber response lies on the slope of the LED emission curve, a shift in the LED spectrum can cause a change in the shape of the spectrum of the probing light and therefore changes the total power transmitted to the sensor detector as compared to the reference detector. If the absorption characteristics of the europium were flat over the transmission band of the filter, then a spectral shift of the probing light would make no difference, since both sensor and reference would see the same shift. In fact, the absorption is not flat. The 610 nm wavelength lies on the slope of the $^7F_2$-$^5D_0$ transition and the absorption decreases fairly strongly with increasing wavelength. If the probe light shifts is spectral shape, it will sample a slightly different portion of the europium absorption and the ratio of incident to transmitted light will change even though there is no actual temperature change in the sensing fiber. We felt that this is the most likely cause of the short-term drift, i.e., the spectrum of the LED's change as they warm up after turn on. It could also be the cause of the long term drift that was observed, if the spectrum of the LED changes as the LED ages.

To check the spectral shift hypothesis measurements at constant probe temperature were taken on the signal outputs from the sensor and reference channel detectors with the RED and IR LED's operating separately. We found that the ratio of the sensor and reference channel signals, which should remain constant, decreased 3 percent during the first five minutes after initiation of the RED LED. The ratio then remained constant during the remaining hour of operation. With the IR LED, the ratio of signals remained constant over the entire hour. These results indicate that it is most likely the spectral change of the RED LED coupled with the spectral passbands of the filter and europium fiber that produces the observable effect on the temperature measurement during the warmup period of the sensor. A detailed measurement of the spectrum of the LED/filter combination and its drift characteristics will be needed, however, to establish with certainty whether it is the cause of the sensor drift.

The performance of the fiber-optic temperature sensor was promising, considering that we could measure a temperature change of $\pm$ 2°C after an initial five minute warmup. With the resolution of the drift problem, the sensor should readily be capable of meeting the goal of 1 percent of point accuracy. Work has been underway with internal sponsorship to help resolve the drift problems and achieve this goal. The following section indicates some promising approaches for further improvement.

5.2   Improvements with Europium Sensor

Unless a much higher brightness, more monochromatic source is used with the europium temperature sensor, we may have to live with a short warm-up period for the sensor output. The warm up drift could be reduced significantly by using a narrower bandpass filter and an LED whose emission spectrum is centered at the europium absorption wavelength. The narrower filter would reduce the optical power. Some of the reduction in power, however, would be made up by centering the LED emission. To choose the most favorable center wavelength and bandwidth for the filters, a series of measurements should be taken to determine the exact way in which the LED spectrum changes relative to the europium spectrum. A trade-off undoubtedly would have to be made between the optical power and bandwidth of the filter. Replacing the LED with a wavelength stable laser source at the europium wavelength, of course, would eliminate the spectral drift problem and give more than adequate light signal levels.

Another improvement that could be made is to use the same focusing optics in the reference channel that we used in the sensor channel. This was originally felt to be unnecessary. Presently, the reference channel collects light directly from the fiber output through the filter. As a consequence, the red reference signal is the weakest. With the placement of identical focusing optics in the reference channel we would increase the red signal level and the overall signal-to-noise ratio. In addition, we would guarantee the same collection angle through the filters in each channel, a possible source of error in itself.

47

As previously mentioned, a small radius europium fiber loop could be made to make a single ended temperature probe (cf, Ref. 1). A single ended probe would allow a better temperature calibration and comparison to a thermocouple sensor. The present large loop probe actually measures an average temperature over the oven used for calibration. The sides of the loop which are near the heating elements in the oven wall may sample a significantly different temperature than the end of the loop where the thermocouple sensor is placed.

A couple other minor improvements would be to place the optics module, oscillator, and signal processing electronics, including the integrators and A/D converters, in a common chassis. This would reduce possible ground loops between the three separate chassis that exist now. It would also be more convenient to place the fiber optic connector at the instrument chassis instead of at the probe.

5.3 Nd Glass Fiber Temperature Sensor

We recently completed spectral measurements vs temperature on a Nd doped YAG crystal. The measurements were made to determine if Nd in YAG would work as a sensor for considerably higher temperatures than the Eu in glass. If the measurements taken on the crystal host have the same validity for a glass host, then Nd in glass would make a better temperature sensor than Eu in glass. First of all, we could use an ir LED. The ir LED's emit over an order of magnitude more optical power than the visible emitting LEDs. Secondly, at certain locations in the spectrum, the sensitivity of the temperature dependent absorption could be improved over that of the Eu in glass. With the Nd, for example, we had some spectral regions where the fiber transmission vs temperature dependence was positive instead of negative. By taking the ratio in two spectral regions that have opposite temperature dependencies, we may be able to improve the sensitivity of the temperature sensor by 50 to 100 percent.

Another feature of Nd that may be an advantage is that at the 1% percent doping levels only a short length of Nd fiber on the order of 1 to 10 mm may be required. This feature allows a higher spatial resolution with the temperature sensor. On the other hand, if an average temperature is required over a long length, the Nd doping level could correspondly by reduced. This is to say, the Nd glass sensor can cover a greater range of spatial resolution than the Eu glass sensor because of the stronger absorption.

48

REFERENCES

1. United Technologies Research Center Monthly Technical Progress Narrative Report, No. R80-924625-10, for NASA Contract NAS3-21841.

2. Monsanto Optoelectronics Applications Guide by William M. Otsuka, September 1978, Monsanto Comapny, Electronics Division.

3. Kawasaki, B. S. and K. O. Hill: Low-Loss Access Coupler for Multimode Optical Fiber Distribution Networks. Appl. Opt. 16, 1794 (1977).

4. Silicon Detector Corporation, "General Purpose Detectors", Form No. 400-44-004.